POLITECNICO MILANO 1863

SCUOLA DI INGEGNERIA INDUSTRIALE E DELL'INFORMAZIONE

Comparative Analysis of Inverter Topologies for Vehicle Wireless Charging based on Efficiency and Control Flexibility

TESI DI LAUREA MAGISTRALE IN
ELECTRICAL ENGINEERING-INGEGNERIA ELETTRICA

Author: **ZHIHAO JIANG**

Student ID: 10968418
Advisor: Morris Brenna
Academic Year: 2025-2026

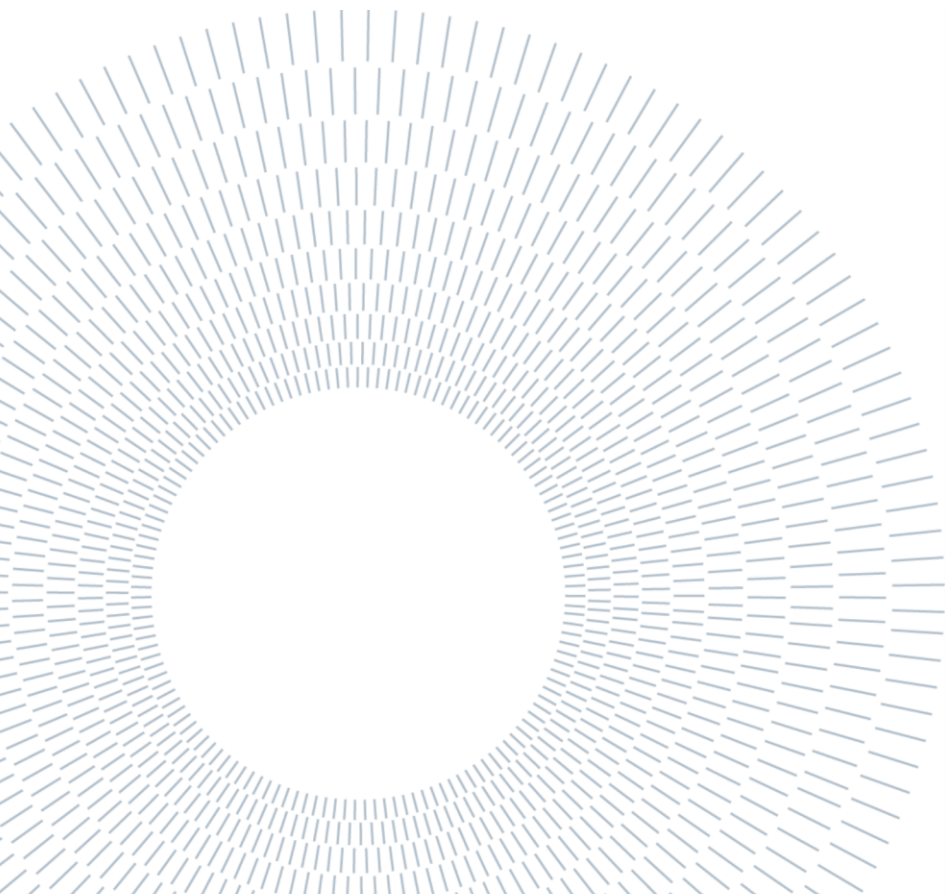

Abstract

With the rapid popularity of electric vehicles (EVs), Wireless Power Transfer (WPT) technology has attracted significant attention due to its convenience, safety, and automation capabilities. However, in practical vehicle applications, the coupling coefficient between transmitting and receiving coils often varies due to parking misalignment. Combined with the nonlinear characteristics of battery loads, this easily leads to a decrease in transmission efficiency and an increase in inverter switching losses.

In this background,This thesis aims to systematically study mainstream inverter topologies and their efficiency optimization control strategies suitable for vehicular WPT systems through theoretical modeling and comparative analysis. Firstly, based on the Fundamental Harmonic Approximation (FHA), equivalent circuit models for mainstream inverters such as Full-Bridge and Half-Bridge under typical resonant networks (e.g., LCC-LCC) are established. Secondly, the theoretical performance of control strategies such as Phase Shift Control (PSC) and Variable Frequency Control (VFC) in achieving Zero Voltage Switching (ZVS) and Maximum Efficiency Point Tracking (MEPT) is deeply analyzed. The regulation capabilities of different control variables against detuning caused by coupler misalignment are also compared.

Finally,Through multi-dimensional theoretical comparative analysis, the results indicate that, in high-power vehicle charging scenarios, the Full-Bridge inverter combined with the LCC-LCC resonant network demonstrates superior soft-switching characteristics and lower device voltage stress over a wide load range. Furthermore, compared with single Variable Frequency Control, the composite control strategy introducing phase shift angle is proven to more effectively maintain high-efficiency operation of the system when the coupling coefficient fluctuates.

Key-words: Electric Vehicles; Wireless Power Transfer; Inverter Topology; Efficiency Optimization; Soft Switching; Theoretical Modeling

Abstract in lingua italiana

Con la rapida diffusione dei veicoli elettrici (EV), la tecnologia di trasferimento di potenza wireless (Wireless Power Transfer - WPT) ha suscitato un notevole interesse grazie alla sua praticità, sicurezza e capacità di automazione. Tuttavia, nelle applicazioni veicolari pratiche, il coefficiente di accoppiamento tra le bobine di trasmissione e ricezione varia spesso a causa del disallineamento in fase di parcheggio. In combinazione con le caratteristiche non lineari del carico della batteria, ciò porta facilmente a una diminuzione dell'efficienza di trasmissione e a un aumento delle perdite di commutazione dell'inverter.

In questo contesto, la presente tesi si propone di studiare sistematicamente le principali topologie di inverter e le relative strategie di controllo per l'ottimizzazione dell'efficienza, adatte ai sistemi WPT veicolari, attraverso la modellazione teorica e l'analisi comparativa. In primo luogo, basandosi sull'Approssimazione della Fondamentale (Fundamental Harmonic Approximation - FHA), vengono stabiliti modelli circuitali equivalenti per gli inverter più diffusi, in presenza di reti risonanti tipiche (ad esempio, LCC-LCC). In secondo luogo, vengono analizzate in modo approfondito le prestazioni teoriche di strategie di controllo come il controllo a sfasamento (Phase Shift Control - PSC) e il controllo a frequenza variabile (Variable Frequency Control - VFC) per il raggiungimento della commutazione a tensione zero (Zero Voltage Switching - ZVS) e del tracciamento del punto di massima efficienza (Maximum Efficiency Point Tracking - MEPT).

Infine, Attraverso un'analisi comparativa teorica multidimensionale, i risultati indicano che, negli scenari di ricarica veicolare ad alta potenza, l'inverter a ponte intero combinato con la rete risonante LCC-LCC dimostra caratteristiche di soft-switching superiori e un minore stress di tensione sui dispositivi in un ampio intervallo di carico.

Parole chiave: Veicoli Elettrici; Trasferimento di Potenza Wireless; Topologia dell'Inverter; Ottimizzazione dell'Efficienza; Soft Switching; Modellazione Teorica.

Contents

1. Introduction

This chapter primarily expounds on the research background and significance of the thesis topic. First, starting from the practical demand for automated charging of electric vehicles, it analyzes the advantages of Wireless Power Transfer (WPT) technology compared to traditional conductive charging, as well as the key technical challenges it faces in vehicular applications, such as coupling mechanism misalignment and non-linear load variations [1].Subsequently, it systematically reviews the current domestic and international research status regarding WPT inverter topologies, resonant compensation networks, and efficiency optimization control strategies, pointing out the deficiencies of existing research in terms of the universality of theoretical modeling and comparative analysis under multiple operating conditions. Finally, the research objectives, main research content, and the overall structural organization of the thesis are clarified.

Furthermore, with the rapid penetration of electric vehicles into the global transportation market, the requirements for charging systems are no longer limited to high power density and conversion efficiency, but also extend to safety, interoperability, electromagnetic compatibility (EMC), and user convenience. In this context, Wireless Power Transfer systems operating typically in the medium-frequency range (tens to hundreds of kilohertz) have emerged as a promising solution, especially for dynamic charging scenarios and autonomous vehicle applications.

Based on the above considerations, this thesis aims to establish a unified analytical framework for comparing different inverter topologies applied in vehicular WPT systems. Through theoretical modeling, operating point analysis, and efficiency-oriented evaluation under multiple coupling and load scenarios, this research seeks to provide quantitative insights into the trade-offs between efficiency performance and control flexibility. The results are expected to contribute to the optimization of inverter selection and control strategy design for next-generation wireless charging systems for electric vehicles.

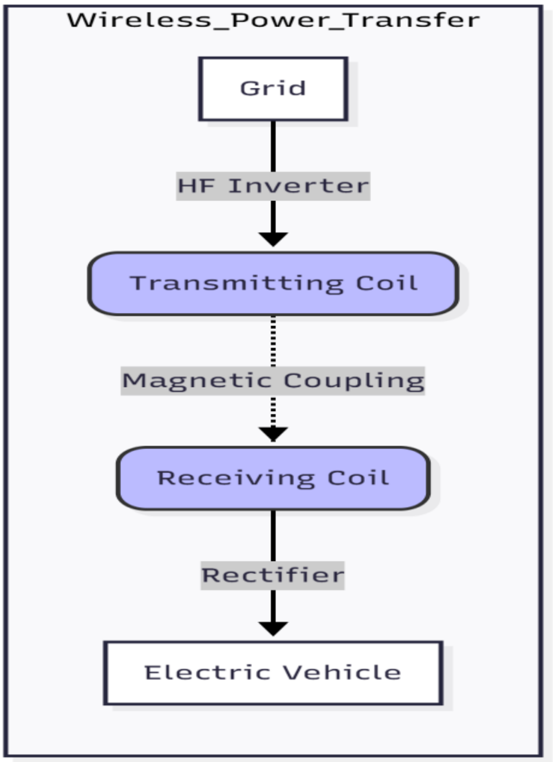

(a)Wireless Power Transfer system

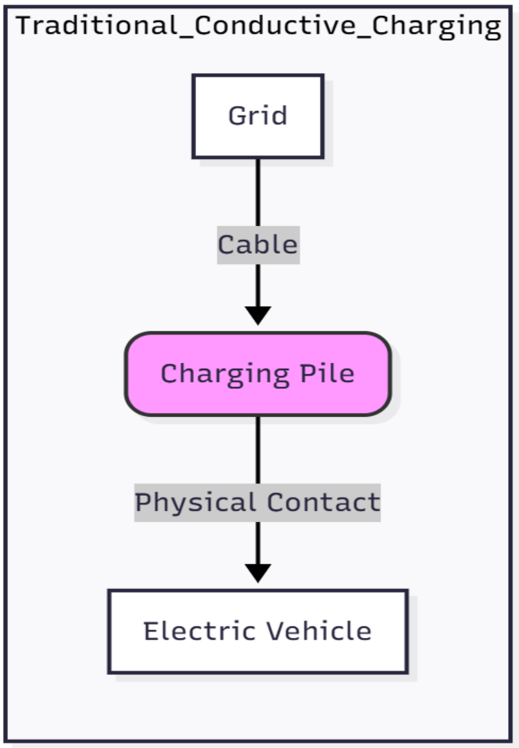

(b)Traditional Conductive Charging system

Figure 1.1: Comparison of Traditional Conductive Charging and Wireless Power Transfer Scenarios.

1.1 Research Background and Significance

To better illustrate the fundamental differences between traditional conductive charging and Wireless Power Transfer (WPT) systems, a conceptual comparison is presented in Figure 1.1. The figure highlights the structural and operational distinctions between the two energy replenishment approaches in vehicular applications. While conventional plug-in charging relies on physical electrical contact between the vehicle and the charging station, WPT systems enable contactless energy transfer through magnetic field coupling. This contrast not only reflects differences in user interaction but also reveals the distinct technical challenges faced by each system architecture.With the automotive industry's profound evolution towards intelligence and unmanned operation, autonomous driving is gradually becoming a reality. In this context, the automation of energy replenishment has become the critical "last mile" to close the loop of the fully autonomous transportation ecosystem [2]. While existing conductive (plug-in) charging technologies are mature, their reliance on manual physical interfaces limits the autonomous capability of vehicles. Furthermore, exposed metal contacts pose safety risks, such as electric sparks and poor contact, under complex conditions like humidity and dust. In contrast, Magnetic Coupled Resonant Wireless Power Transfer (MCR-WPT) technology completely eliminates physical electrical connections. Due to its flexibility, safety, and inherent electrical isolation, it is universally recognized as the optimal charging solution for future Electric Vehicles (EVs) and the technological cornerstone for realizing dynamic ("charge-as-you-go") wireless charging [3].

However, transitioning WPT technology from laboratories to large-scale vehicular applications faces unique technical bottlenecks distinct from wired charging. The most pressing challenge is the extreme sensitivity of transmission efficiency to positional misalignment [4]. In practical parking scenarios, due to driver habits or errors in automatic parking systems, lateral or angular misalignment between the transmitting and receiving coils is inevitable. This geometric randomness causes the Coupling Coefficient (k) of the system to fluctuate over a wide range.For the High-Frequency Inverter, which acts as the "heart" of the WPT system, such parameter fluctuations are critical. When the coupling mechanism is detuned, the inverter often deviates from its optimal operating point, leading to:

1. Loss of Soft-Switching (ZVS/ZCS) Conditions: Switching devices degrade into hard-switching modes, resulting in massive switching losses and severe overheating;
2. Drop in Transmission Power: Inability to meet the charging demands of the battery;
3. Excessive Electromagnetic Stress: Resonant currents may surge instantaneously, endangering the safety of power devices.

Traditional constant-frequency or single-variable control strategies struggle to cope with such wide-range parameter perturbations. Therefore, investigating how to optimize the inverter's topology and control logic to "lock" onto the maximum efficiency point and maintain soft-switching operation—even under the dual disturbances of non-ideal coil alignment and non-linear battery load variations—is the key to enhancing the practicality of vehicular WPT systems. This research is pivotal not only for energy utilization efficiency but also for determining the volume, thermal management costs, and lifespan of On-Board Chargers (OBC), holding significant engineering value [5].

1.2 Literature Review

To address the challenges, academia and industry have conducted extensive research on the core technologies of WPT systems.

1.2.1 Research on Inverter Topologies

The inverter is responsible for converting DC bus voltage into high-frequency AC to drive the resonant network. Currently, the Full-Bridge Inverter is the mainstream choice for high-power vehicle charging due to its high-power capacity and control flexibility. Half-bridge inverters also hold a place in low-to-medium power applications due to their simplicity. Recently, to further improve efficiency, resonant converters such as LLC and CLLC topologies have received widespread attention [6]. The CLLC topology with its symmetric resonant network structure, naturally supports bidirectional energy flow, making it highly suitable for wireless charging applications. Additionally, advanced topologies like Modular Multilevel Converters (MMC) show excellent performance in wired chargers, but their application in vehicular wireless systems is still exploring. To provide a clearer structural understanding of the vehicular wireless power transfer system and its associated power conversion stages, the overall system architecture and representative inverter topologies are illustrated in Figure 1.2.

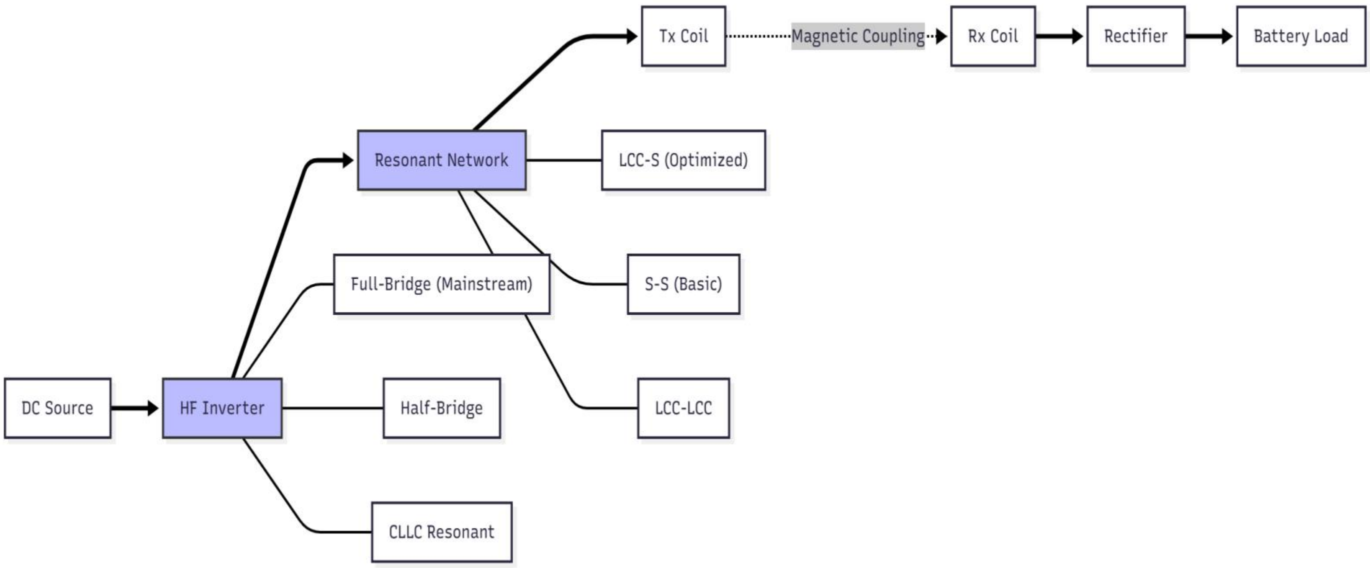

Figure 1.2: WPT System Architecture and Mainstream Topology.

1.2.2 Research on Efficiency Optimization Control Strategies

To mitigate the detuning effects caused by coupling misalignment and load variations, the optimization of control strategies is paramount. While Variable Frequency Control (VFC) is commonly employed to track the resonant point for soft switching, its effective regulation range is severely constrained by international standards (e.g., SAE J2954) [7], which strictly limit the operating frequency band to 81.38 – 90 kHz. Alternatively, Phase Shift Control (PSC) offers a simpler, fixed-frequency solution; however, it is prone to losing Zero Voltage Switching (ZVS) conditions under light loads or significant coil misalignment [8], resulting in a sharp decline in efficiency. Consequently, current research hotspots have shifted towards Composite Control Strategies that integrate both frequency and phase modulation. These hybrid approaches aim to overcome the limitations of single-variable control, thereby achieving Maximum Efficiency Point Tracking (MEPT) and maintaining robust performance across a wide operating range.

1.2.3 Limitations of Existing Research

Although existing literature has deeply analyzed specific topologies, there is a lack of systematic theoretical comparison of different inverter topology and control strategy combinations under unified vehicular operating conditions. Most research relies on specific experiments, lacking a universal mathematical model to rapidly evaluate the robustness of different schemes under parameter perturbations.

1.3 Research Objectives and Content

Guided by the overarching goal of enhancing the technical feasibility and operational reliability of high-power wireless charging systems, the investigation undertaken within the framework of this dissertation centers primarily upon a deep theoretical exploration of the LCC-LCC resonant topology. This research prioritizes rigorous analytical derivation over immediate hardware prototyping. The comprehensive research contents are strategically organized into the following three distinct yet interconnected dimensions:

1. Precise Mathematical Modeling and Steady-State Characteristic Analysis: In view of the intricate electromagnetic interactions inherent in high-order resonant networks, it is imperative to establish a robust analytical framework. By directing specific analytical attention toward the LCC-LCC resonant network (illustrated in Figure 1.3), which has emerged as a predominant paradigm in contemporary vehicular charging infrastructures, this work seeks to transcend simplified assumptions.

Meticulous equivalent circuit models for both Full-Bridge and Half-Bridge inverters are established through the systematic application of the widely recognized Fundamental Harmonic Approximation (FHA) method, which provides an optimal balance between computational efficiency and analytical accuracy [9]. This exhaustive derivation process yields high-fidelity analytical expressions for input impedance, voltage gain, and device-level current stress. By examining these metrics under a spectrum of varying coupling coefficients and load conditions, the research establishes an indispensable theoretical cornerstone that facilitates a more profound comprehension of subsequent system behaviors [10];

2. Design and Synthesis of Adaptive Efficiency Optimization Control Strategies: Against the backdrop of the performance imperatives delineated in the design targets of Table 1.1, the maintenance of peak efficiency across a highly dynamic operational range remains a significant challenge. This section delves into the multi-objective optimization problem by conducting a thorough comparative study of the regulation characteristics of Phase Shift Control (PSC) and Variable Frequency Control (VFC). To navigate the complexities of real-world charging environments, a synergistic Maximum Efficiency Point Tracking (MEPT) hybrid control logic is proposed, specifically designed to adapt autonomously to wide-range coupling variations [11];
3. Construction and Comparative Analysis of Performance Evaluation System: A multi-dimensional evaluation model, including transmission efficiency, device stress, and robustness, is established. Using MATLAB/Simulink, the LCC-LCC topology's performance is quantitatively verified. The simulation focuses on validating the system's ability to maintain efficiency and a stable current even when subjected to 20% coupling fluctuations and significant load variations, providing practical engineering recommendations for WPT system design.

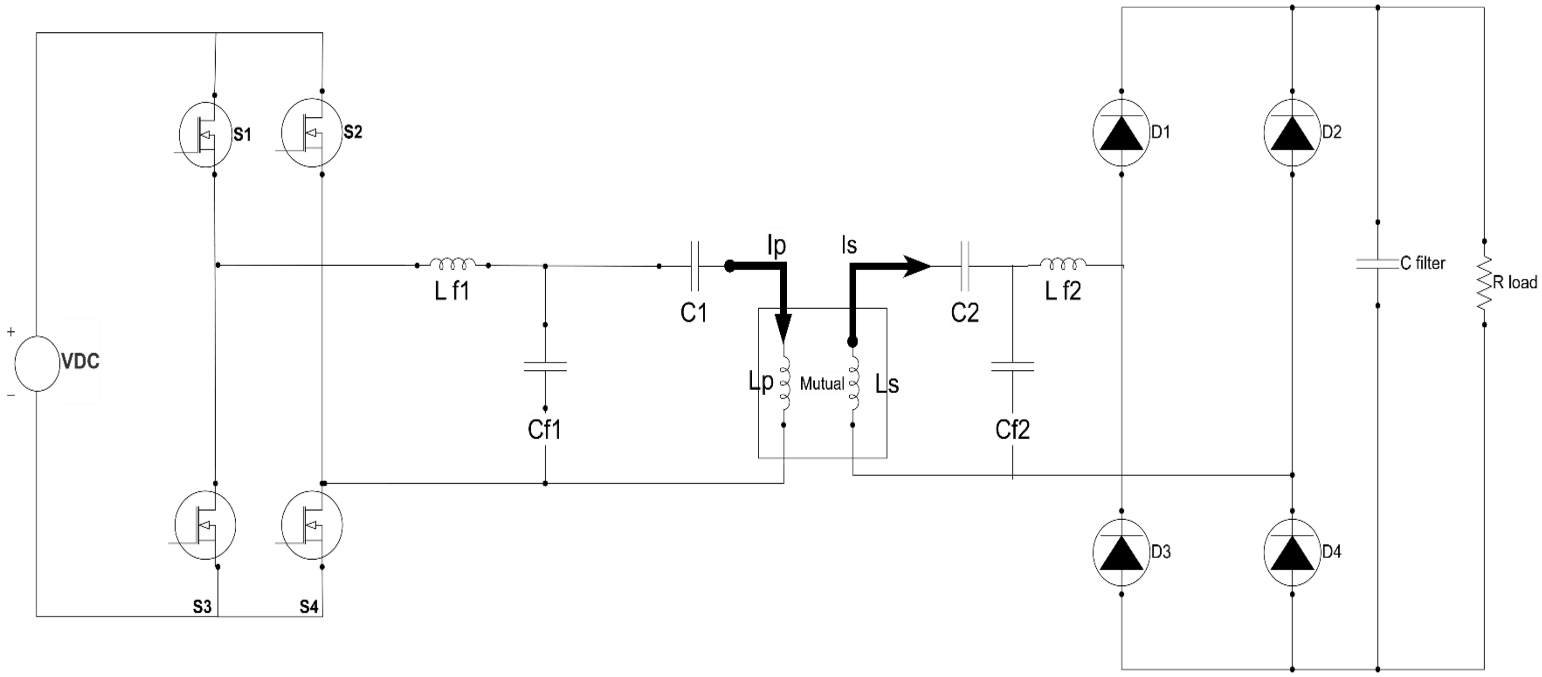

Figure 1.3: LCC-LCC Topology.

Evaluation Dimension	**Key Metrics**	**Optimization Goal**
Efficiency Performance	System Transmission Efficiency (η)	Achieve greater than 82% across the full load range.
Soft-Switching Characteristics	ZVS / ZCS Implementation Range	Maintain Zero Voltage Switching (ZVS) condition even under coupling coefficient (k) fluctuations.
Component Stress	Peak Switch Voltage(V_{peak}) & Current (I_{peak})	Minimize electrical stress to reduce device rating requirements and cost.
Control Characteristics	Algorithm Complexity & Response Speed	Implement a dual-loop control feasible for real-time processing.
System Robustness	Tolerance to Coupling Variation (Δk)	Maintain stable operation under ±20% parking misalignment

Table 1.1: Performance Evaluation for Vehicular WPT Inverters.

1.4 Thesis Organization

To systematically present the aforementioned research, the structure of this thesis is

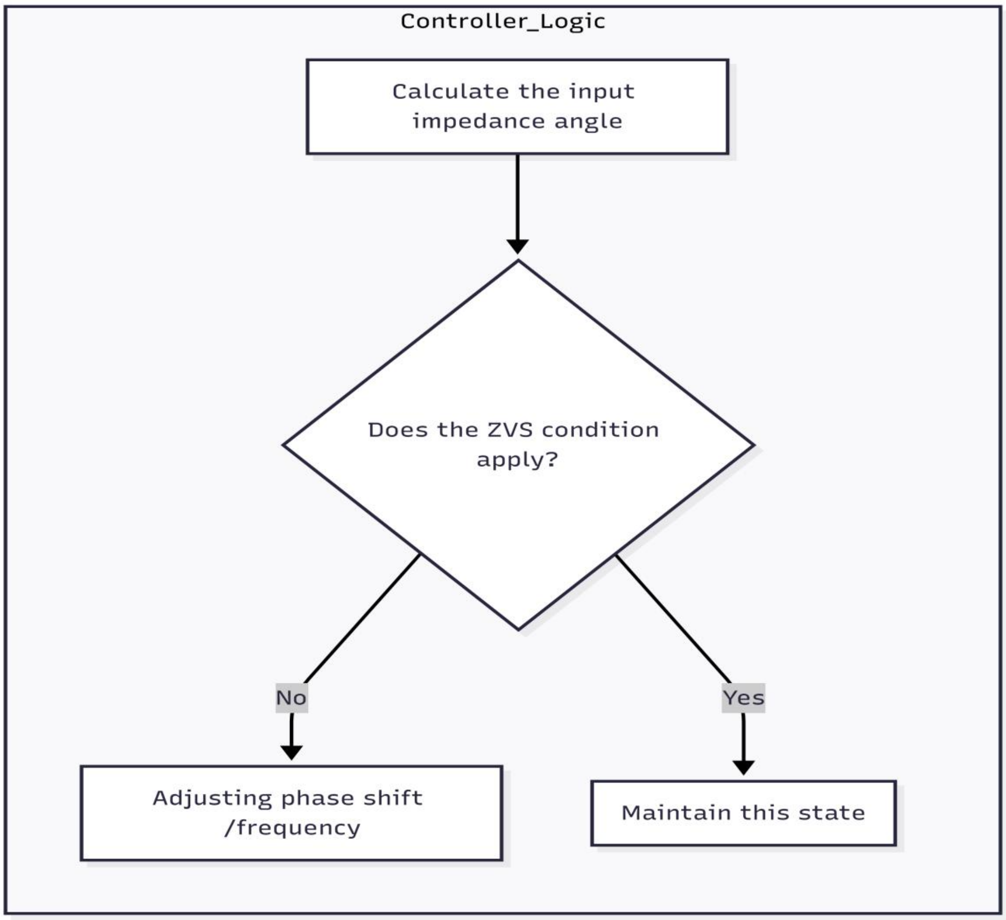

Figure 1.4: Diagram of Inverter Control Logic Based on MEPT.

organized as follows: Based on the theoretical framework and research objectives outlined in the previous sections, this thesis is structured in a progressive and logically coherent manner. Each chapter is designed to build upon the analytical foundation established earlier, gradually transitioning from fundamental system principles to inverter modeling, control strategy optimization, and comprehensive performance evaluation. The overall organization aims to ensure both theoretical rigor and engineering applicability, aligning with the central research theme of enhancing efficiency and control flexibility in vehicular wireless power transfer systems.

Chapter 1: Introduction. Expounds on the background and significance of EV wireless charging, summarizes the domestic and international research status on inverter topologies and control strategies, and points out existing deficiencies, leading to the research objectives of this thesis. Chapter 2: Fundamentals of Wireless Power Transfer Systems. Analyzes the working mechanism of magnetic resonant WPT systems, focusing on the circuit characteristics of the LCC-LCC resonant compensation network and its requirements for the inverter. Chapter 3: Theoretical Modeling of Mainstream Inverter Topologies. Derives in detail the mathematical models of Full-Bridge and Half-Bridge inverters, establishing the quantitative relationship between input impedance and system parameters. Chapter 4: Research on Efficiency Optimization Control Strategies. Analyzes the impact of different control variables on system efficiency and designs a Maximum Efficiency Point Tracking (MEPT) control flow based on theoretical models. As illustrated in Figure 1.4, the proposed MEPT-based control architecture serves as the central methodological framework of this study. The subsequent chapters are therefore organized to progressively derive, validate, and evaluate this control structure from both theoretical and simulation perspectives. Chapter 5:Comprehensive Comparative Analysis. Based on the mathematical models derived earlier, compares the robustness and efficiency performance of different schemes under parameter perturbations through numerical calculation. Chapter 6: Conclusion and Future Work. Summarizes the main conclusions and innovations of the thesis and provides an outlook on future research directions.

Through this structured progression, the thesis forms a closed analytical loop: beginning with system-level challenges, advancing through rigorous mathematical modeling and control optimization, and culminating in quantitative comparative validation. This organization ensures that the proposed inverter topology analysis and MEPT-based control strategy are not only theoretically justified but also practically validated under realistic vehicular operating conditions.

2. Basic Principles of Wireless Power Transfer System

2.1 Introduction

This chapter introduces the basic principles of wireless power transfer (WPT) systems. It begins with a brief review of the technological background and development trends of wireless power transfer. The chapter then elaborates on the structure and working principle of the magnetic-coupled resonant wireless power transfer (MCR-WPT) system. By analyzing the various components of the system, the mutual inductance model and its equivalent circuit are discussed. The chapter focuses on the analysis of the LCC-LCC resonant compensation network, providing theoretical foundations for the design and optimization of inverters in subsequent chapters.

2.2 Magnetic-Coupled Resonant WPT System Structure

Wireless power transfer systems involve a complex, multi-stage energy conversion process. First, the DC input at the ground end is converted into alternating current by a high-frequency inverter. Then, resonance is achieved through a primary compensation network, enhancing the magnetic field emission capability. Energy is coupled to the secondary coil via the magnetic field in the air gap, and then converted back into DC power to supply the battery load via the secondary compensation network and rectifier circuit [12]. In this process, the inverter's switching frequency is typically set at around 85kHz (compliant with SAE J2954 standard). The overall system efficiency depends heavily on inverter loss control and the matching of the primary and secondary resonant states [13].

A typical magnetic-coupled resonant wireless power transfer (MCR-WPT) system mainly consists of a DC power supply, high-frequency inverter, resonant compensation network, loosely coupled transformer (transmitting and receiving coils), rectification and filtering circuits, and load .The basic energy flow process is as in Figure 2.1 follows:

1. High-Frequency Inverter Stage: The grid input AC is first rectified to DC, then converted into high-frequency AC square wave voltage through a high-frequency inverter. This stage is crucial for enhancing transmission efficiency and is the core focus of this study;
2. Resonant Coupling Stage: To compensate for the reactive power generated by the leakage inductance of the coils, resonant compensation networks are introduced on both the transmitting and receiving sides. The high-frequency current excites the transmitting coil to generate an alternating magnetic field, and through magnetic coupling, induces electromotive force in the receiving coil, enabling contactless energy transfer;
3. Rectification Output Stage: The high-frequency AC received by the receiving coil is passed through the secondary compensation network, then converted into stable DC through a rectifier bridge and filter capacitors. This DC is finally supplied to an electric vehicle's power battery or other loads.

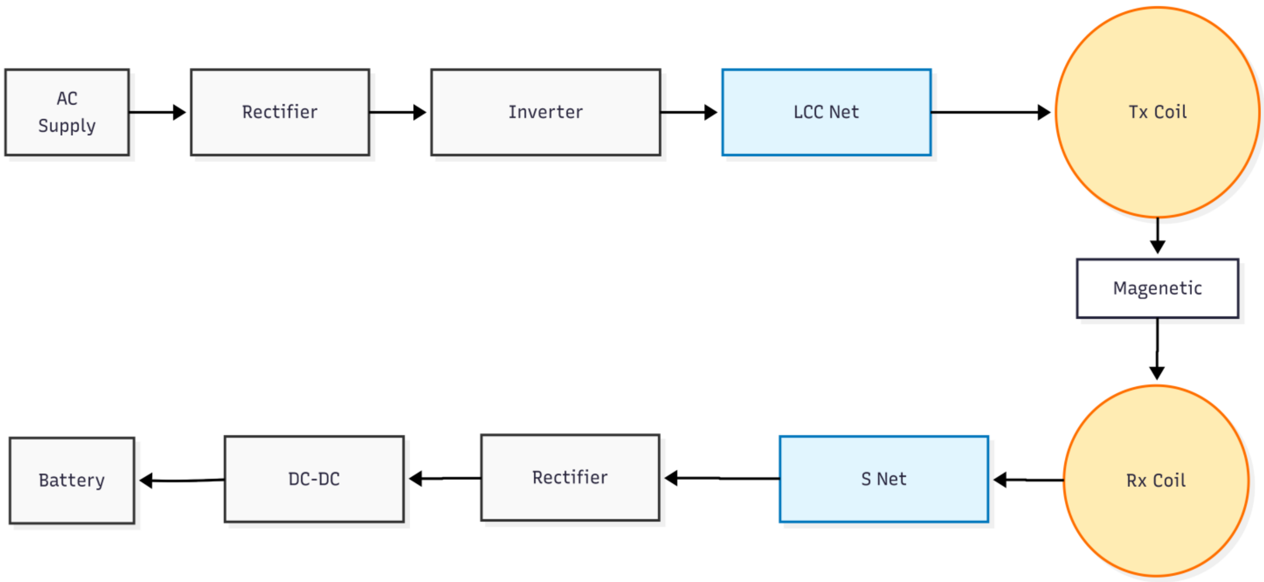

Figure 2.1: Block diagram of WPT system.

2.3 Analysis of Mutual Inductance Model

Mutual inductance models are a core tool for analyzing loosely coupled transformers. By introducing the mutual inductance coefficient M and the coupling coefficient k, the complex spatial magnetic field problem can be transformed into circuit parameters. In this chapter, we analyze the voltage and current phasor relationships between the primary and secondary coils using an equivalent T-type circuit model [14], which lays the theoretical foundation for establishing the full-parameter mathematical model of the LCC-LCC system in Chapter 3.

In wireless power transfer systems, the LCT(Loose Coupling Transformer) is the core component for enabling wireless energy transfer. Unlike traditional transformers, there is a significant air gap between the primary and secondary coils of the LCT, which means the magnetic circuit is not closed, resulting in high leakage inductance and low coupling coefficient. For ease of circuit analysis, mutual inductance models or T-type equivalent circuit models are commonly used. Let the inductance of the transmitting coil be Lp, the inductance of the receiving coil be Ls, and the mutual inductance between them be M [15]. According to Kirchhoff's Voltage Law (KVL), the voltage-current relationship across the coils can be expressed as:

$$\begin{cases} \dot{U}_p = jwL_p\dot{I}_p - jwM\dot{I}_s, \\ \dot{U}_s = jwM\dot{I}_p - jwL_s\dot{I}_s. \end{cases} \tag{2.1}$$

Here, ω represents the system's operating angular frequency (ω=2πf), $\dot{U}_p$ and $\dot{U}_s$ are the voltage phasors across the primary and secondary coils, respectively, $\dot{I}_p$ and $\dot{I}_s$ are the current phasors. The coupling coefficient k describes the degree of magnetic coupling between the two coils, and it is defined as:

$$\{ k = \frac{M}{\sqrt{L_p L_s}}. \tag{2.2}$$

In the application of wireless charging for electric vehicles, due to the limitations of the chassis height and the presence of parking misalignment, the coupling coefficient k typically ranges between 0.1 and 0.3. This weak coupling characteristic means that the system must rely on a resonant compensation network to counteract the large reactive power generated by the leakage inductance, thereby enhancing the power transfer capability. This is precisely the reason for introducing the LCC-LCC resonant network in the next section.

2.4 Analysis of the LCC-LCC Resonant Compensation Network Characteristics

In the architecture of high-power inductive power transfer (IPT) systems, resonant compensation networks serve a critical function by neutralizing the large leakage inductance inherent in loosely coupled transformers. This compensation is essential for minimizing the reactive power circulation within the system and significantly enhancing the overall power factor and efficiency. While traditional Series-Series (SS) topologies have gained popularity due to their structural simplicity, they often exhibit a heightened sensitivity to load fluctuations, leading to undesirable frequency bifurcation and stability issues in dynamic charging environments.

In contrast, the double-sided LCC (LCC-LCC) compensation topology has emerged as a superior benchmark for high-power electric vehicle (EV) charging applications. By integrating additional inductive and capacitive filtering elements on both the transmitting and receiving sides, the LCC-LCC network facilitates a high degree of decoupling between the output power and the magnetic coupling variations. Most importantly, this topology is uniquely characterized by its inherent load-independent constant current (CC) output characteristic [16]. As established in the strategic goals of this thesis, maintaining a stable current charging current is paramount for the initial bulk charging stage of EV batteries, as it ensures a controlled energy transfer rate and prevents battery degradation. Consequently, the LCC-LCC configuration was selected as the rigorous research benchmark for this investigation.

Regarding the power conversion stage, current research into 3.3 kW vehicular wireless power transfer (WPT) systems emphasizes that the Full-Bridge (FB) inverter demonstrates substantial technical superiority over the traditional Half-Bridge (HB) configuration. The primary advantages of the FB topology reside in its enhanced power-handling capacity and operational control flexibility [17]. From a voltage utilization perspective, under an identical DC bus voltage, an FB inverter is capable of delivering twice the peak-to-peak AC output voltage compared to its HB counterpart. As a direct mathematical consequence, to achieve the same target power throughput, the root-mean-square (RMS) current flowing through the FB circuit is effectively halved. This significant reduction in current magnitude mitigates conduction losses in the power MOSFETs and alleviates the thermal stress imposed on the resonant components and coupling coils, thereby optimizing the thermal stability and power density of the fast-charging system.

Furthermore, in terms of control versatility, the FB topology introduces an indispensable degree of freedom: Phase-shift Control (PSC). Unlike HB inverters, which are largely constrained to Frequency Modulation (FM) for power regulation, a method that often forces the system to operate far from its optimal resonant point—the FB inverter allows for precise regulation by modulating the phase-shift angle between its two bridge arms. This capability enables the system to maintain a stable operating frequency near the resonance, improving robustness against parking misalignments and extending the region for achieving Zero Voltage Switching (ZVS).

To facilitate a rigorous analysis of the steady-state transmission characteristics, the Fundamental Harmonic Approximation (FHA) method is systematically employed. As illustrated in the detailed circuit diagram in Figure 1.3, the LCC-LCC topology investigated in this work utilizes a symmetric and sophisticated compensation structure. On the transmitting side, the primary LCC network consists of a series filter inductor L_{f1}, a parallel filter capacitor C_{f1}, and a series compensation capacitor C_1. Correspondingly, on the receiving side, instead of a simple series capacitor, an LCC composite compensation network is implemented, comprising a secondary filter inductor L_{f2}, a parallel capacitor C_{f2}, and a series compensation capacitor C_2. This dual-LCC configuration is essential for achieving the multi-objective performance targets defined in the subsequent theoretical derivations.

2.4.1 Resonance Conditions and Parameter Matching

In order to minimize the reactive power circulation and maximize the overall energy conversion efficiency, the WPT system is strategically designed to operate in a resonant state, ensuring that the inverter’s output voltage and current remain substantially in phase. For the double-sided LCC (LCC-LCC) topology discussed in this research, the parameter matching process is significantly more complex than that of traditional single-side compensation networks. The design of the system's resonant angular frequency, ω_{res}, assuming $\omega = \omega_{res}$ for idealized analysis is predicated on the synchronized resonance of four distinct reactive branches across both the transmitting and receiving sides [18].Firstly, to achieve a stable and load-independent Constant Current (CC) output—a critical requirement for the initial stage of EV battery charging—the primary-side and secondary-side filtering branches must satisfy the fundamental resonance relationship. The filtering inductors Lf1 and Lf2 must resonate with their respective parallel capacitors Cf1 and Cf2 at the target operating frequency in equation (2.3)

$$\omega = \frac{1}{\sqrt{L_{f1}C_{f1}}} = \frac{1}{\sqrt{L_{f2}C_{f2}}} \tag{2.3}$$

Here, This specific matching condition ensures that the current flowing through the transmitting coil (L_p) and the receiving coil (L_s) is decoupled from the load variations, providing the theoretical basis for stable charging current observed in subsequent simulations.Secondly, to fully compensate for the self-inductance of the coupling coils and ensure a purely resistive input impedance at the resonance point, the series compensation capacitors C_1 and C_2 must be precisely tuned. Unlike the simple series compensation where the capacitor directly matches the coil inductance, in an LCC-LCC configuration, the values of C_1 and C_2 are intrinsically linked to the difference between the coil inductance and the filtering inductance. Specifically, they must satisfy the following parameter matching conditions in equation (2.4), Where L_p represents the self-inductance of the primary transmitter coil and L_s denotes the self-inductance of the secondary receiver coil. By satisfying these dual-side matching relationships, the reactive components of the leakage flux are effectively neutralized. This allows the system to maintain a high power factor and enables the inverter to achieve Zero Voltage Switching (ZVS) through slight inductive detuning, as further analyzed in the frequency-domain modeling section.

$$\begin{cases} C_1 = \dfrac{1}{\omega^2(L_P - L_{f1})}, \\ C_2 = \dfrac{1}{\omega^2(L_s - L_{f2})}. \end{cases} \tag{2.4}$$

2.4.2 Input Impedance Analysis

The input impedance characteristics of the resonant network represent a fundamental bridge between the power electronic stage and the magnetic coupling stage. This parameter is the decisive factor in determining the operational trajectory of the inverter’s switching devices (S_1-S_4), as it dictates the phase relationship between the fundamental voltage and current. In a double-sided LCC-LCC wireless power transfer system, the complexity of the impedance derivation increases due to the higher order of the resonant tank. According to the mutual inductance coupling theory, the secondary-side network, which includes the receiver coil and its LCC compensation elements—imposes a reflected load onto the primary transmitter coil. This interaction is mathematically described by the reflected impedance Z_{ref}. For the LCC-LCC configuration, the impedance Z_{ref} reflected from the secondary loop into the primary coil is defined as equation(2.5):

$$Z_{ref} = \frac{\omega^2 M^2}{Z_{total}} \tag{2.5}$$

Where M is the mutual inductance and Z_{total} represents the comprehensive impedance of the secondary resonant loop. After meticulous mathematical simplification, when the system operates precisely at the designed resonant frequency ω and strictly adheres to the parameter matching conditions established in the preceding section, the total input impedance Z_{in} as equation (2.6) will exhibit purely resistive characteristics [19].

$$Z_{in} = j\omega L_{f1} + (\frac{1}{j\omega C_{f1}}||(j\omega L_p + \frac{1}{j\omega C_1} + Z_{ref})) \tag{2.6}$$

This state implies that the phase angle between the inverter's output voltage and current is zero, minimizing the circulation of reactive power. While this purely resistive characteristic is a critical theoretical benchmark, it is often marginally adjusted in practical control strategy designs to enhance system reliability. If the operating switching frequency is maintained slightly higher than the natural resonant frequency in a practical implementation, the input impedance will transition into a weakly inductive behavior. This shift causes the inverter output current to lag behind the voltage by a specific phase interval. This lagging phase relationship is a necessary condition for achieving Zero Voltage Switching (ZVS) of the MOSFET switching devices (S_1-S_4) [20].During the dead-time period, this inductive current facilitates the charging and discharging of the MOSFETs' parasitic output capacitances, ensuring that the voltage across the switch drops to zero before the gate-drive signal is applied. By systematically designing the impedance to stay within this inductive region, the turn-on switching losses are effectively eliminated, thereby optimizing the thermal performance and long-term stability of the 3.3 kW high-power inverter.

2.5 Summary

This chapter has provided a systematic and in-depth analytical investigation into the operational mechanisms and theoretical foundations of magnetic coupling resonant wireless power transfer (WPT) systems. By establishing a rigorous mathematical and physical framework, the research has laid the necessary groundwork for the subsequent design of advanced control strategies and performance optimization. The key contributions and findings of this chapter can be summarized as follows:

Firstly, a comprehensive system-level block diagram was constructed, encompassing the grid-side rectification, the high-frequency Full-Bridge inverter stage, the magnetic coupling resonator, and the onboard receiver modules. This systemic visualization served to clarify the complex energy flow relationships and power conversion stages between the individual modules, ensuring a holistic understanding of the 3.3 kW power transfer trajectory.

Secondly, utilizing Kirchhoff's circuit laws and mutual inductance coupling theory, a high-fidelity equivalent circuit model of the loosely coupled transformer was established. This modeling approach allowed for the precise analysis of the physical principles underlying non-contact power transfer, particularly focusing on the electromagnetic interactions between the primary transmitter and secondary receiver coils under various coupling conditions. Finally, the input impedance characteristics were analyzed to determine the boundary conditions for efficient power conversion. It was theoretically demonstrated that while the system exhibits purely resistive input impedance at the exact resonant point, a slight inductive detuning is required to facilitate Zero Voltage Switching (ZVS). This analysis provides the indispensable theoretical support for the mathematical modeling of the Full-Bridge inverter and the implementation of the efficiency-optimized control strategies that will be explored in the forthcoming chapters.

Finally, the input impedance characteristics were analyzed to determine the boundary conditions for efficient power conversion. It was theoretically demonstrated that while the system exhibits purely resistive input impedance at the exact resonant point, a slight inductive detuning is required to facilitate Zero Voltage Switching (ZVS). This analysis provides the indispensable theoretical support for the mathematical modeling of the Full-Bridge inverter and the implementation of the efficiency-optimized control strategies that will be explored in the forthcoming chapters.

3. Modeling and Characteristic Analysis of Inverter Topologies

In the previous chapter, the overall architecture of the Magnetically Coupled Resonant Wireless Power Transfer (MCR-WPT) system was established, and the circuit characteristics and mutual inductance coupling mechanism of the LCC-LCC resonant compensation network were elaborated in detail. However, as the core link of energy conversion in the system, the operating state of the high-frequency inverter directly determines the transmission efficiency, electromagnetic interference level, and operational stability of the switching devices.

Different inverter topologies and their control methods result in distinct output voltage harmonic contents and soft-switching characteristics. In order to deeply investigate the performance of inverters in high-power vehicular applications, this chapter establishes mathematical models of mainstream inverter topologies from a theoretical perspective.

This chapter first takes the classic full-bridge inverter as an example, analyzing its output voltage in both time and frequency domains using Fourier Series. This study uses the Fundamental Harmonic Approximation (FHA) method combined with phasor analysis. The rationale for this method is that higher-order compensation networks such as LCC-LCC have natural bandpass filtering characteristics, which can effectively filter out higher harmonics, so that the energy exchange of the system is mainly carried by the fundamental component [22]. Through this modeling method, we can simplify the nonlinear inverter output into a controlled sinusoidal voltage source, thereby clearly revealing the theoretical boundary between inverter topology, resonant parameters and transmission efficiency. Subsequently, combining the impedance characteristics of the LCC-LCC resonant network, the boundary conditions and parameter constraints for achieving Zero Voltage Switching (ZVS) of the inverter are derived. Finally, an efficiency evaluation model based on loss analysis is established. These theoretical derivations avoid tedious experimental trial-and-error, providing rigorous mathematical support and a theoretical basis for the optimization of control strategies in subsequent chapters.

3.1 Analysis of Full-Bridge Inverter Topology

The Voltage-Source Full-Bridge Inverter is one of the most mature and widely used topological structures in high-power wireless power transfer (WPT) systems. Its primary function is to convert the DC input voltage into a high-frequency AC square wave voltage to drive the subsequent resonant network. Due to its simple structure, low voltage stress on switching devices, and ease of implementing soft-switching control.

3.1.1 Circuit Structure and Operating Principle

The primary power conversion architecture of the proposed WPT system is founded upon a high-frequency Full-Bridge (FB) inverter, the AC equivalent analysis model of which is meticulously illustrated in Figure 3.1. This topology is strategically chosen for high-power applications (3.3 kW) due to its superior voltage utilization and control flexibility. The inverter bridge is composed of four power MOSFETs (labeled S_1,S_2,S_3,S_4), each integrated with an anti-parallel body diode to provide a freewheeling path for the inductive current during dead-time intervals. As depicted in the schematic, the four switches are organized into two symmetric bridge legs: the leading leg consists of S_1 and S_3, while the lagging leg is formed by S_2 and S_4. The DC input voltage source, Vdc, supplies the bridge, and the intricate LCC-LCC resonant network is connected between the bridge midpoints A and B. Unlike simpler configurations, the load network here is not a singular impedance but a high-order resonant tank comprising the primary compensation elements (L_{f1}, C_{f1}, C_1) and the magnetically coupled secondary LCC structure. This sophisticated arrangement is crucial for filtering high-order harmonics from the inverter output and ensuring a near-sinusoidal current I_p in the transmitter coil.

Crucially, the switching frequency f_s is maintained at 86 kHz (aligned with the industry standards while allowing for inductive detuning). This fixed-frequency operation is a key physical basis for maintaining the system near its optimal resonant point, even when confronted with power instabilities caused by parking position deviations or significant load fluctuations. Furthermore, as will be derived in the subsequent mathematical modeling, the interaction between the phase-shift angle and the LCC-LCC network's inductive impedance creates the necessary conditions for achieving Zero Voltage Switching (ZVS), thereby optimizing the conversion efficiency and mitigating thermal stress on the power devices [23].

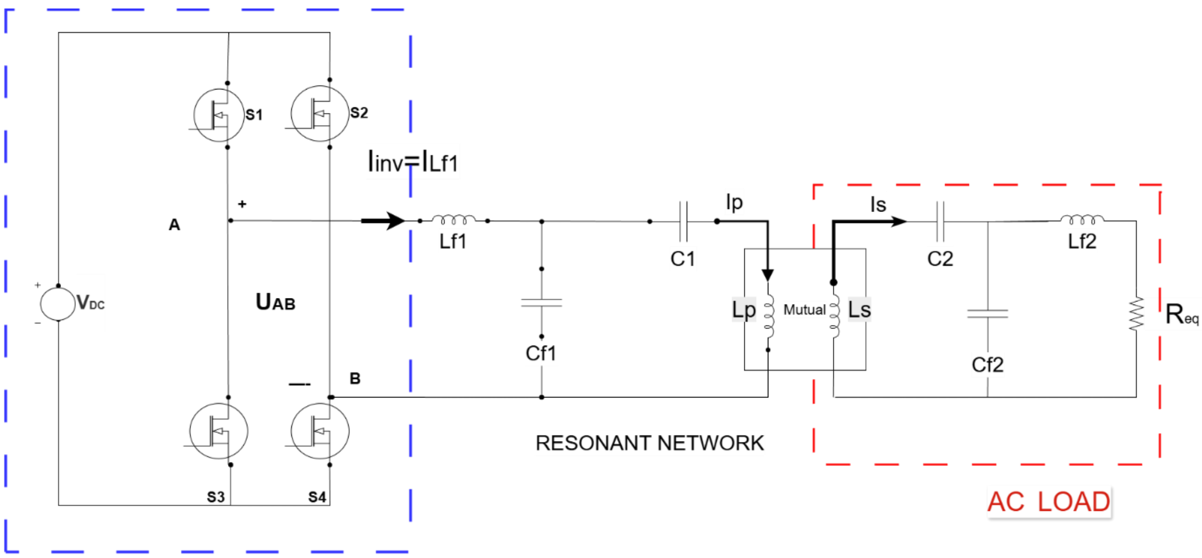

Figure 3.1: AC Equivalent Analysis Model of Full-Bridge Inverter and Resonant Network.

3.1.2 Mathematical Modeling of Full-Bridge Inverter Output Voltage

To conduct a rigorous analytical investigation into the operational characteristics of the wireless power transfer system, it is imperative to establish a precise mathematical representation of the excitation source. The high-frequency Full-Bridge (FB) inverter, acting as the primary energy conversion unit, generates a high-frequency AC carrier from the DC input. This paper implements the Phase Shift Control (PSC) strategy, a sophisticated modulation technique that regulates the effective output voltage—and consequently the transmitted power—by manipulating the relative temporal displacement between the driving signals of the two inverter legs. Based on established methodologies in mainstream literature [1, 5, 12], the fundamental control parameters are defined as follows: Vdc: The constant DC bus input voltage. ω_s : It is important to note that while the system is designed to operate near resonance, the excitation frequency is fundamentally determined by the switching signals of the H-bridge. Therefore, we define as the operating angular frequency of the inverter represents the actual switching angular frequency imposed by the controller. Phase Shift Angle ϕ:Defined as the phase angle by which the lagging leg delays the leading leg. with a range of 0 ⩽ ϕ ⩽ ⊓.Pulse Width Angle δ: This corresponds to the angle of the duration for which the output voltage U_AB is non-zero within a half-cycle. Its relationship with the phase shift angle is complementary:

$$\delta = \pi - \phi \tag{3.1}$$

Frequency Domain Analysis: Ignoring the conduction voltage drop and dead time of the switching devices, the inverter output voltage U_{AB} is a three-level stepped wave with an amplitude of $\pm V_{DC}$ Expanding it using Fourier Series, and considering the odd symmetry of the waveform，we get (3.3).Substituting equation(3.1) into the above equation and using the trigonometric identity (3.2)for odd n, the output voltage expression(3.4) can be expressed as a function of the phase shift angle ϕ.

$$\begin{cases} \sin(n\dfrac{(\pi-\phi)}{2}) = \cos(\dfrac{n\phi}{2}), & (3.2) \\ U_{AB}(t) = \displaystyle\sum_{n=1,3,5\ldots}^{\infty} \dfrac{4V_{dc}}{n\pi}\sin(\dfrac{n\delta}{2})\sin(n\omega_s t), & (3.3) \\ U_{AB}(t) = \displaystyle\sum_{n=1,3,5\ldots}^{\infty} \dfrac{4V_{dc}}{n\pi}\cos(\dfrac{n\phi}{2})\sin(n\omega_s t). & (3.4) \end{cases}$$

Fundamental Harmonic Approximation: A significant attribute of the LCC-LCC resonant compensation network is its exceptional frequency selectivity and filtering capability. Because the high-order resonant tank presents extremely high impedance to higher-order harmonics, the system energy is overwhelmingly carried by the fundamental frequency component. Therefore, this research employs the

Fundamental Harmonic Approximation (FHA) for all subsequent theoretical derivations. By extracting the n=1 component from Equation (3.4), the inverter output fundamental voltage $U_{AB,1,(t)}$ and its RMS value U_{inv} are obtained:

$$\begin{cases} U_{AB,1}(t) = \dfrac{4V_{dc}}{\pi}\cos(\dfrac{\phi}{2})\sin(\omega_s t), \\ U_{inv} = \dfrac{2\sqrt{2}V_{dc}}{\pi}\cos(\dfrac{\phi}{2}). \end{cases} \tag{3.5}$$

Conclusion: From Equation (3.5) [24], it is evident that the inverter output fundamental voltage U_{inv} is directly proportional to the cosine of half the phase shift angle ϕ.When $\phi = 0$, $\delta = \prod$, the output is a full square wave, and the fundamental voltage is maximized.When $\phi = \prod$, $\delta = 0$, the output voltage is turned off. This mathematical model not only accurately describes the output characteristics of the inverter but also clarifies the physical basis for achieving constant voltage/constant current output control by regulating ϕ.

3.2 Impedance Characteristic Analysis of LCC-LCC Resonant Network

Following the establishment of the mathematical model for the inverter output voltage, this section performs a detailed frequency-domain modeling of the double-sided LCC resonant compensation network as illustrated in the equivalent circuit of Figure 3.1. The LCC-LCC architecture is characterized by its high-order reactive components, which provide superior filtering and impedance transformation capabilities. Specifically, the transmitting side comprises a primary filter inductor L_{f1}, a parallel capacitor C_{f1}, and a tuning capacitor C_1. Correspondingly, the secondary side is configured with a tuning capacitor C_2, a parallel capacitor C_{f2}, and a secondary filter inductor L_{f2}. To facilitate a manageable analytical process while preserving the core physical characteristics of the power transfer, the following assumptions are established based on the Fundamental Harmonic Approximation (FHA):

- All inductive and capacitive elements are treated as ideal lossless components during the initial impedance derivation, with parasitic resistances neglected (these are reintroduced in the efficiency and thermal stress analysis in Chapter 5).
- The operating frequency is assumed to be maintained in the vicinity of the system's natural resonant frequency ω_0.

- The non-linear rectifier bridge, subsequent filtering stages, and the battery load are collectively represented as a pure equivalent AC resistance, R_{eq}.

The analytical derivation begins at the secondary (receiving) side. Unlike a simple series-compensated receiver, the LCC structure on the secondary side acts as an impedance transformer. The secondary resonant loop interacts with the transmitter coil through the mutual inductance M [16]. According to the mutual inductance coupling theory, the impedance of the secondary network is reflected back to the primary transmitter coil L_p. In a tuned LCC-LCC system, when the secondary parameters satisfy the resonance condition, the reflected impedance Z_{ref} can be derived. Under the condition where L_{f2} resonates with C_2, the reflected impedance is purely resistive at the resonant frequency and can be expressed as equation(3.7):

$$Z_{ref} = \frac{\omega^2 M^2 R_{eq}}{L_{f2}^2 \omega^2} = \frac{M^2 R_{eq}}{L_{f2}^2}. \tag{3.7}$$

The equivalent impedance Zin of the primary circuit is the key basis for designing Soft Switching (ZVS) of the inverter. Viewing from the inverter output terminals (Points A and B) towards the load, the input impedance of the LCC network consists of the Lf1 branch in series with the "C_f parallel branch". The parallel branch is formed by C_{f1} in parallel with the series branch, which consists of C_1, L_p, and the reflected impedance Zref.Therefore, the expression for the total system input impedance Zin as(3.8),Expanding and rearranging yields as (3.9) [22].

$$\begin{cases} Z_{\text{in}} = j\omega L_{f1} + \dfrac{1}{j\omega C_{f1}} \,||\, (\dfrac{1}{j\omega C_1} + j\omega L_p + Z_{ref}), & (3.8) \\ Z_{in} = j\omega L_{f1} + \dfrac{Z_{ref} + j\omega L_p + \dfrac{1}{j\omega C_1}}{1 + j\omega C_{f1}[Z_{ref} + j\omega L_p + \dfrac{1}{j\omega C_1}]}. & (3.9) \end{cases}$$

A significant characteristic of the LCC compensation network is the "constant current source" behavior of its transmitting coil current [25]. To verify this, it is necessary to derive the transmission relationship between the transmitting coil current Ip and the inverter output voltage U_{inv}.Define the parallel branch impedance Z_{branch} (3.10)of the back-end and the series impedance Z_{series}(3.11)of the transmitting branch.According to Kirchhoff's Voltage Law (KVL) and the current divider rule, the current Ip flowing through the transmitting coil L_P can be expressed as(3.13):When the system parameters satisfy the LCC resonance condition (L_{f1} resonates with C_{f1} at the switching frequency, $\omega^2 L_{f1} C_{f1} = 1$) [26], the above formula can be significantly simplified as(3.14).

$$Z_{branch} = \frac{1}{j\omega C_{f1}} || (\frac{1}{j\omega C_1} + j\omega L_p + Z_{ref}), \tag{3.10}$$

$$Z_{series} = j\omega L_p + \frac{1}{j\omega C_1} + Z_{ref}, \tag{3.11}$$

$$I_{inv} = \frac{U_{inv}}{Z_{inv}} = \frac{U_{inv}}{j\omega L_{f1} + Z_{branch}}, \tag{3.12}$$

$$I_p = I_{inv} \cdot \frac{\frac{1}{j\omega C_{f1}}}{Z_{series} + \frac{1}{j\omega C_1}} = \frac{U_{inv}}{j\omega L_{f1} + Z_{branch}} \cdot \frac{1}{1 + j\omega C_{f1} Z_{series}}, \tag{3.13}$$

$$I_p = \frac{U_{inv}}{j\omega L_{f1}}, \tag{3.14}$$

$$I_{out} = \frac{M \cdot U_{inv}}{\omega L_{f1} L_{f2}}. \tag{3.15}$$

Conclusion Analysis: Two important conclusions can be drawn from Equation (3.14), the magnitude of the transmitting coil current I_P depends only on the input voltage U_{inv} and the primary inductance L_{f1}, and is independent of the load impedance. Furthermore, for the Double-Sided LCC topology, the output current I_{out} is proportional to the primary current I_P. By substituting the secondary circuit equations, the output current can be expressed as (3.15):This characteristic is of great significance for the subsequent analysis of system power transmission and control strategies.

3.2.1 Analysis of Conditions for Achieving Zero Voltage Switching (ZVS) in Full-Bridge Inverters

Symbol	Parameter	Value
V_{in}	DC Input Voltage	300 V
f_s	Operating Frequency	86 kHZ

f_{res}	Resonant Network Tuning Frequency	84 kHZ
P_{out}	Rated Output Power	3.3 KW
L_{f1}	LCC Series Inductance	35 μH
C_{f1}	LCC Parallel Capacitance	97.85 nF
C_1	Primary Series Capacitance	17.12 nF
L_p	Transmitter Coil Inductance	235 μH
L_s	Receiver Coil Inductance	235 μH
C_2	Secondary Series Capacitance	17.12 nF
M	Mutual Inductance	42 μH
R_{eq}	Equivalent Load Resistance Range	10~500 Ω
t_d	dead time	600 ns
C_{par}	MOSFET Output Capacitance	600 pF
C_{f2}	Secondary LCC Parallel Capacitance	97.85 nF
L_{f2}	Secondary LCC Series Inductor	35 μH

Table 3.1: Key Circuit Parameters of the LCC-LCC System.

To verify the soft-switching characteristics of the LCC-LCC topology, a simulation model was constructed in this paper. The main circuit parameters of the system (including coil inductance and mutual inductance) were referenced from the experimental prototype data in reference [27]. Based on this, to ensure zero-voltage switching (ZVS) of the full-bridge inverter, the operating frequency was intentionally designed to be slightly higher than the resonant frequency of the compensation network. This inductive detuning strategy guarantees that the input impedance of the resonant tank presents an inductive characteristic at the switching frequency, thereby allowing the resonant current to flow in the appropriate direction during the dead-time interval. During the dead-time period, the resonant current charges and discharges the MOSFET output capacitances, naturally reducing the switch voltage (Vds) to nearly zero before the corresponding gate signal turns on. Simulation results confirm that Vds reaches approximately zero prior to the rising edge of the gate signal, indicating successful ZVS operation under rated load conditions.Therefore, the combined effect of inductive detuning and properly selected dead-time ensures reliable ZVS operation of the full-bridge inverter. The final key system parameters are shown in Table 3.1.

In high-power vehicular wireless charging systems, the switching loss of the high-frequency inverter is one of the main sources of total system loss. To improve system efficiency and reduce the temperature rise of the switches, it is essential to ensure that the inverter operates in a Zero Voltage Switching (ZVS) state. This section quantitatively analyzes the boundary conditions for achieving ZVS in full-bridge inverters, combining the input impedance model derived in Section 3.2.

3.2.2 Physical Mechanism and Necessary Conditions for ZVS

The MOSFET switches in a full-bridge inverter typically have parallel parasitic capacitances C_{par} (or external snubber capacitors). The essence of ZVS is to use the inductive current in the load loop to extract the charge from the parallel capacitor before the switch turn-on signal arrives, causing the voltage across it to drop to zero (or be clamped by the anti-parallel diode), thereby achieving "zero voltage" turn-on.

Therefore, two necessary conditions must be met to achieve ZVS:Firstly,Inductive Input Impedance: The inverter output current I_{inv} must lag the output voltage U_{AB} in phase. This means the total input impedance Z_{in} of the resonant network must be inductive, its imaginary part $Im(Z_{in}) > 0$.Secondly,Sufficient Turn-off Current: During the dead time t_d, the current flowing through the switch must be large enough to completely discharge the junction capacitor C_{par}. The physical mechanism of ZVS relies on the inductive energy stored in the primary resonant tank to discharge the drain-source capacitance of the MOSFETs during the dead-time [27].

3.2.3 ZVS Region Analysis Based on Input Impedance Angle

Define the system's input impedance angle θ_{in} as the phase angle of the input impedance Z_{in}. According to Equation (3.9), θ_{in} can be expressed as (3.16):

$$\theta_{in} = \arctan(\frac{\mathrm{Im}(Z_{in})}{\mathrm{Re}(Z_{in})}). \tag{3.16}$$

To ensure the inverter operates in the inductive region, the condition $\theta_{in} > 0$ must be satisfied.

For the LCC-LCC topology, when the system operates exactly at the resonant frequency ω_0, theoretically Z_{in} is purely resistive ($\theta_{in} = 0$). Although the power factor is highest at this point, it fails to meet the requirement for inductive current needed for ZVS, easily leading to hard switching.

Therefore, in practical engineering design, the inverter's operating frequency fs is usually set slightly higher than the system's natural resonant frequency f_0, or the

LCC network parameters are adjusted to make the system appear slightly inductive at the rated operating point.

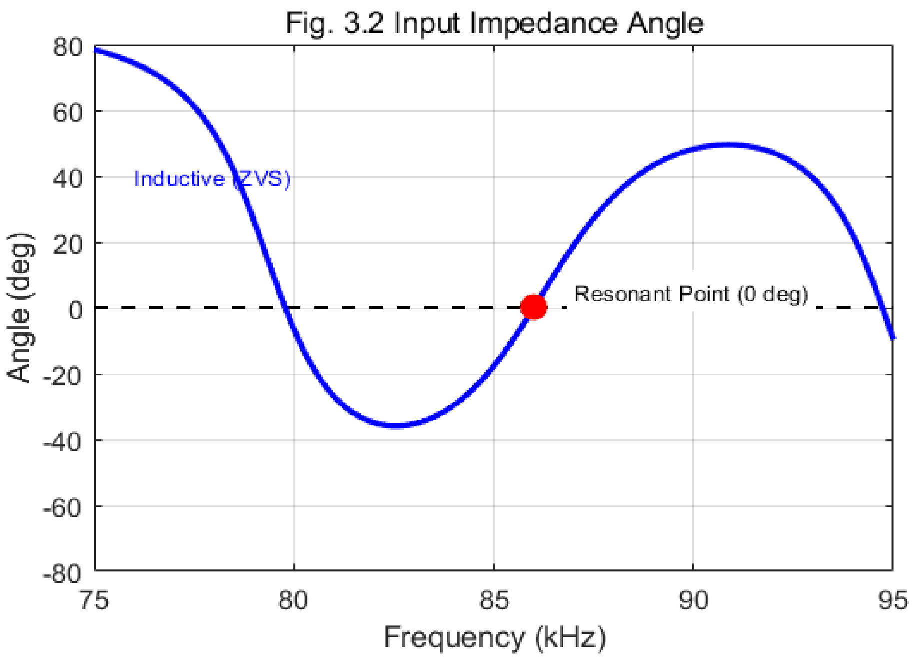

Figure 3.2: Input Impedance Angle.

Figure 3.2 shows the simulated characteristic curve of the system input impedance angle θ_{in} as a function of frequency. The impedance angle curve crosses zero precisely at the resonance point of 84 kHz. To the left of this frequency (f < 84 kHz), the network exhibits capacitive characteristics; to the right (f > 84 kHz), it exhibits inductive characteristics. This paper selects 86 kHz as the rated frequency, where At this frequency, the input impedance angle is approximately 25° . This positive angle indicates that the input voltage leads the current, and the inductor has sufficient energy storage. This satisfies the freewheeling current requirement after MOSFET turn-off, achieving reliable ZVS, while avoiding excessive reactive power loss caused by an excessively large impedance angle (θ_{in}>60°), thus achieving a balance between soft switching and transmission efficiency.

3.2.4 Mathematical Inequality for ZVS Realization

To ensure the charging and discharging of C_{par} is completed within the dead time t_d, the inductor current I_{off} at the turn-off moment must satisfy the energy condition as (3.17):

$$\frac{1}{2}L_{eq}I_{off}^2 > C_{eq}V_{dc}^2. \tag{3.17}$$

Where $C_{eq} = 2C_{par}$ is the equivalent capacitance of the bridge leg. Combined with phase shift control, when the phase shift angle is ϕ, achieving ZVS for the lagging leg is typically more difficult than for the leading leg. To ensure soft switching over the full range, the system design must guarantee that the inductive component of the input impedance maintains sufficient freewheeling current even under conditions of minimum load and maximum phase shift angle.

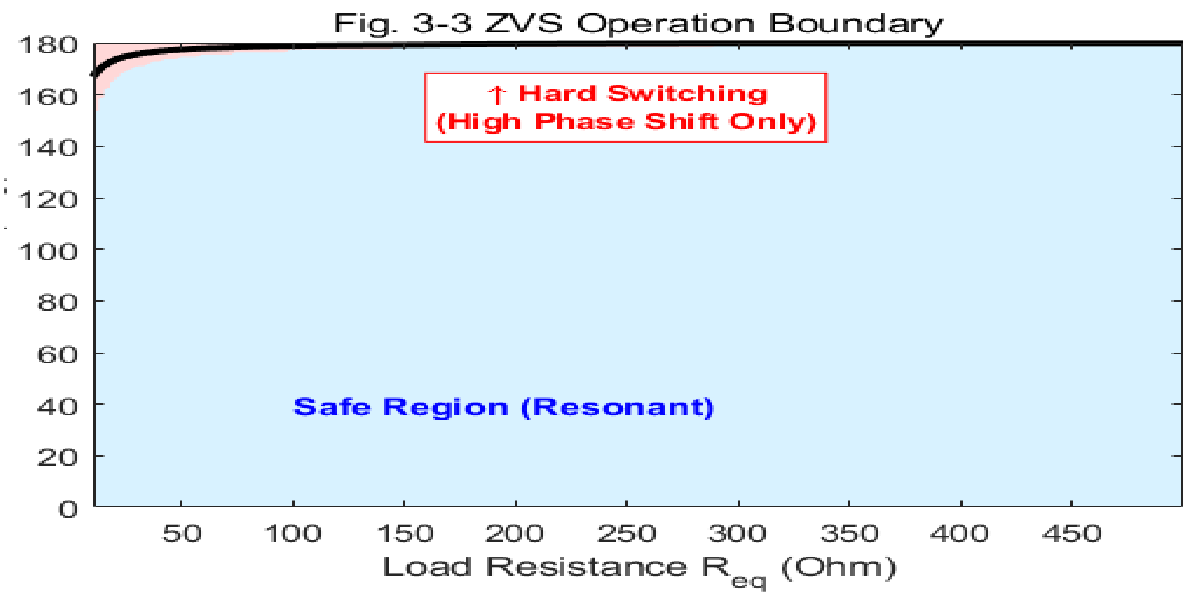

Figure 3.3: ZVS Operation Boundary under Variable Load and Phase Shift.

Conclusion: Figure 3.3 shows the ZVS operating boundary scan diagram of the system at the rated operating frequency (86 kHz). In the figure, the blue area represents the "safe region" that meets the soft switching conditions, the red area represents the "hard switching" region, and the black solid line is the critical boundary between the two. As established in [28], the ZVS region is essentially defined by the boundaries of the input phase angle. To maintain ZVS across the 3.3 kW power range, the system must operate in a slightly inductive region where the reactive power is sufficient for commutation. From the above analysis, the parameter design of the LCC-LCC network must not only consider constant current output but also require fine-tuning (such as slightly decreasing C_f) to keep the input impedance angle θ_{in} within a small positive range (typically 10° ~20°). This ensures ZVS operation across the full load range [29].

3.3 Analysis of Constant Current Output Characteristics of LCC-LCC System

This section presents a comprehensive evaluation of the steady-state output performance of the designed bilateral LCC wireless power transfer system. The objective is to validate whether the hardware parameters selected in the previous sections can fulfill the rigorous charging requirements of electric vehicle batteries. Initially, a formal mathematical derivation based on coupled-circuit theory is performed to elucidate the physical mechanism behind the inherent constant current (CC) property of the LCC-LCC topology. Subsequently, a high-fidelity simulation model is constructed using the parameters established in Table 3.1 (Lf1=Lf2=35 μH). By conducting a parametric sweep of the load resistance, the stability and accuracy of the output current are quantified to ensure reliable operation across a broad load spectrum.

3.3.1 Theoretical Derivation of Constant Current Output

As detailed in the impedance analysis in Section 3.2, the Double-Sided LCC resonant network exhibits inherent constant current (CC) source characteristics when operating at the resonant frequency. According to the derived Equation (3.15), the output current I_{out} is expressed ,This analytical expression indicates that the output current magnitude is solely determined by the system design parameters (U_{inv},ω,M,L_{f1},L_{f2}) and is strictly independent of the load resistance R_{eq}. Therefore, theoretically, the system can maintain a stable charging current throughout the constant-current charging stage of the battery, regardless of the variation in equivalent load resistance. The following simulation aims to verify this theoretical characteristic under the designed parameters [30].

3.3.2 Simulation Verification of Output Characteristics

To verify the theoretical constant current capability, a simulation sweep was conducted based on the optimized parameters listed in Table 3.1 (L_{f1}=L_{f2}=35μH). The system was set to operate at the strict resonant frequency (f_s = 86 KHz), and the load resistance R_{eq} was varied from 10 Ω~200 Ω to simulate the charging process.

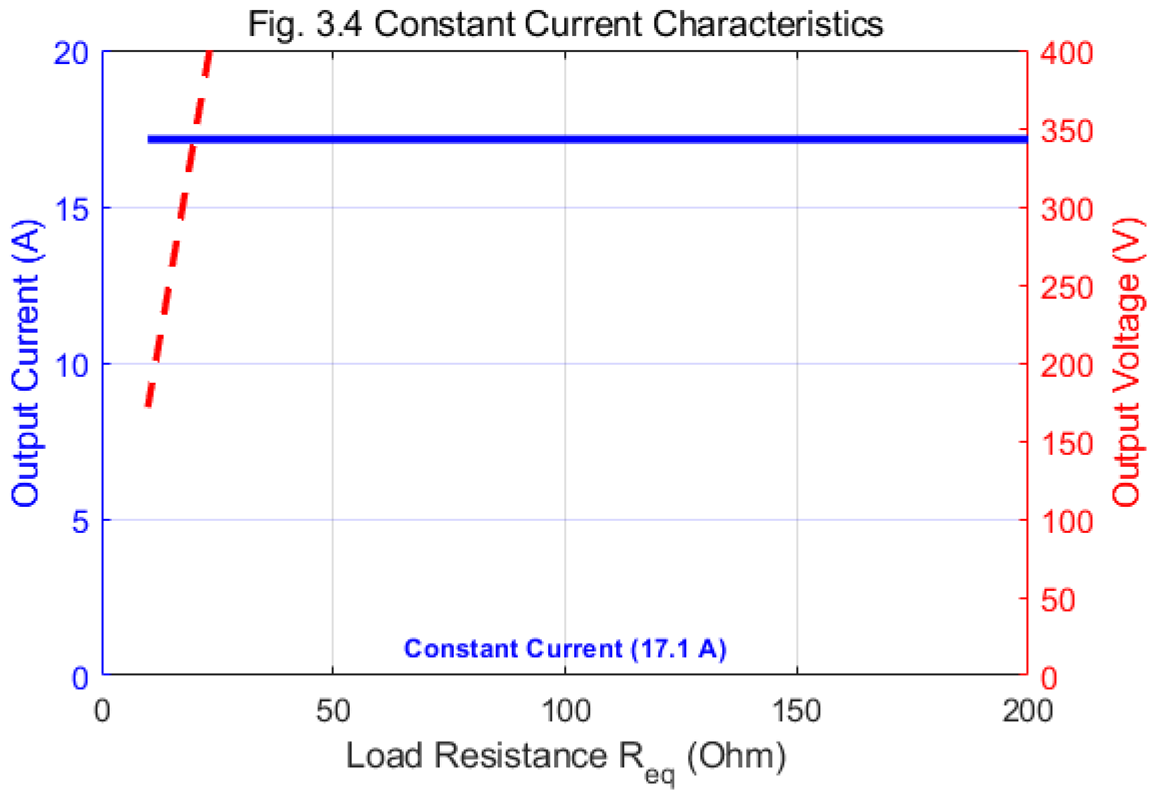

Figure 3.4: Constant current Characteristics.

The simulation results can be analyzed as follows: Firstly, Constant Current Regulation: As indicated by the solid blue trajectory, the output current remains exceptionally stable at approximately 17.1 A throughout the entire load range. The curve demonstrates remarkable linearity and flatness, with negligible deviation from the theoretical prediction of 17.1 A. This confirms that the LCC-LCC topology, with the designed 35 μH inductors, functions as a near-ideal current source. Secondly, Voltage Proportionality: The dashed red line depicts the output voltage, which exhibits a linear increase in direct proportion to the load resistance. This behavior aligns with Ohm's Law ($V_{out}=I_{out}\cdot R_{eq}$), which is the standard operational signature of a constant current excitation source.

In conclusion, the simulation results provide robust evidence that the selected parameter set successfully achieves the 3.3 kW target power level while maintaining a stabilized 17.1 A output, validating the effectiveness of the LCC-LCC design.

3.4 Summary

This chapter presented a comprehensive theoretical analysis and simulation verification of the main circuit characteristics for the Double-Sided LCC wireless power transfer system. The key contributions and conclusions of this chapter are summarized as follows:

Circuit Modeling and Parameter Design: The fundamental T-model equivalent circuit of the Double-Sided LCC topology was established. Based on the resonance theory, the key circuit parameters were calculated and optimized, with the series inductors (L_{f1},L_{f2}) designed at 35μH to satisfy the required power and current levels.

Impedance Characteristics Analysis: The frequency-domain analysis of the input impedance demonstrated that the system operates at a strict resonant state at the switching frequency of 86 KHz. The input impedance angle is zero, ensuring a unity power factor and minimizing reactive power circulation, which is beneficial for system efficiency.

ZVS Operation Boundary: The conditions for achieving Zero Voltage Switching (ZVS) were analyzed. The simulation identified the "Safe Region" and "Hard Switching Region" under different load resistances and phase shift angles. The results confirm that the Double-Sided LCC topology exhibits excellent soft-switching robustness, particularly under light-load conditions.

Output Characteristics Verification: Theoretical derivation and simulation results verified the inherent constant current output characteristic of the system. The system maintains a stable output current of approximately 17.1 A across a wide load range (10Ω~200Ω), validating the effectiveness of the parameter design.

In conclusion, the theoretical analysis and simulation results in this chapter confirm that the designed main circuit possesses stable constant current output capability and good soft-switching performance. These characteristics provide a solid hardware foundation for the closed-loop control strategy design in Chapter 4.

4. Research on Inverter Efficiency Optimization Control Strategy

In the previous chapter, the theoretical modeling and characteristic analysis of the inverter topologies for vehicle wireless charging systems were conducted, establishing the resonant converter as the preferred main circuit topology. However, optimizing hardware parameters alone is insufficient to guarantee system performance across the full load range. especially when the equivalent load changes during battery charging or when the coil coupling varies, the system efficiency often drops significantly. Therefore, it is of great significance to maintain the high-efficiency operation of the inverter through advanced control strategies.This chapter first establishes a detailed mathematical loss model of the inverter based on the physical characteristics of power devices to identify the key factors affecting efficiency. Secondly, it analyzes the working principles of Phase Shift Control (PSC) and Frequency Control and their impacts on Zero Voltage Switching (ZVS) characteristics. Finally, a Maximum Efficiency Point Tracking (MEPT) control strategy combining phase shift and frequency modulation is proposed, aiming to achieve optimal efficiency output under parameter variations.

4.1 Loss Analysis Model of the Inverter

To achieve optimal control of inverter efficiency, a quantitative analysis of its energy loss mechanism is a prerequisite. Under the high-frequency operating conditions of vehicle wireless charging systems, the power losses of the inverter are mainly generated by power semiconductor switches (MOSFETs) and exhibit a nonlinear coupling relationship with parameters such as load current, switching frequency, and junction temperature. Based on the physical switching characteristics of power devices, the total loss of the inverter is typically decomposed into static conduction loss and dynamic switching loss. This section will establish mathematical models for these two parts respectively [31], thereby deriving the total loss function of the inverter, which provides a theoretical basis for establishing the objective function for maximum efficiency control.

4.1.1 Loss Composition Analysis

In the vehicle wireless power transfer (WPT) system, the high-frequency inverter serves as the core unit for energy conversion, and its efficiency directly determines the performance of the transmitter side. Based on semiconductor physics, the power losses of the inverter are mainly generated by the power switches (MOSFETs), which are specifically divided into two parts: conduction loss (P_{con}) and switching loss (P_{sw}). To achieve closed-loop control for efficiency optimization, establishing an accurate mathematical model of losses is crucial.

4.1.2 Conduction Loss Model

Conduction loss is the Joule heat generated due to the on-state resistance $R_{ds(on)}$ of the switches during conduction. For a full-bridge inverter, two diagonal switches are always conducting simultaneously at any given operating moment. Therefore, the total conduction loss of the inverter can be expressed as:

$$P_{con} = 2 \cdot I_{rms}^2 \cdot R_{ds(on)} \tag{4.1}$$

Where I_{rms} is the root mean square (RMS) value of the current flowing through the switch (which is equivalent to the RMS value of the inverter output current I_{inv}), and $R_{ds(on)}$ is the on-resistance of the power MOSFET . It is worth noting that $R_{ds(on)}$ increases with the rise of junction temperature T_j; thus, the temperature coefficient must be considered in practical calculation [32].

4.1.3 Switching loss model and soft switching analysis

Switching loss occurs during the transient intervals of turn-on and turn-off. In traditional hard-switching, the overlap of the drain-source voltage and drain current leads to significant dissipation. However, the LCC-LCC topology ensures that the inverter operates in a Zero Voltage Switching (ZVS) state by maintaining a slightly inductive input impedance. Under ZVS conditions, the voltage across the switch is clamped to zero by the anti-parallel diode before it turns on; therefore, the turn-on loss (P_{on}) is approximately zero. Consequently, the switching loss of the inverter mainly consists of turn-off loss [33], and its mathematical model can be approximated as:

$$P_{sw} \approx P_{off} = 4 f_s \cdot E_{off} \tag{4.2}$$

Where f_s is the switching frequency, and E_{off} is the energy dissipation per turn-off event, which is positively correlated with the turn-off current I_{off} and the DC bus voltage V_{dc}.

4.1.4 Total inverter losses

Synthesizing the above analysis, the total power loss of the inverter P_{loss} can be expressed as the sum of conduction loss and switching loss, Since two diagonal switches conduct simultaneously at any given moment in a full-bridge inverter, and all four switches undergo a turn-off event within one switching cycle (assuming ZVS is achieved and turn-on loss is negligible), the total loss model can be mathematically formulated as:

$$\begin{cases} P_{loss} = P_{con} + P_{sw}, & (4.3) \\ P_{loss} = 2I_{rms}^2 R_{ds(on)} + 4f_s \cdot E_{off}. & (4.4) \end{cases}$$

This model indicates that to maximize system efficiency, the control strategy should aim to find the optimal operating point to reduce I_{rms} and E_{off} while meeting the power transfer requirements,Specifically, the optimization objectives are:Reducing the reactive circulating current component by optimizing impedance matching,And Lowering the turn-off current to reduce E_{off}, provided that the minimum current requirement for Zero Voltage Switching (ZVS) is met.

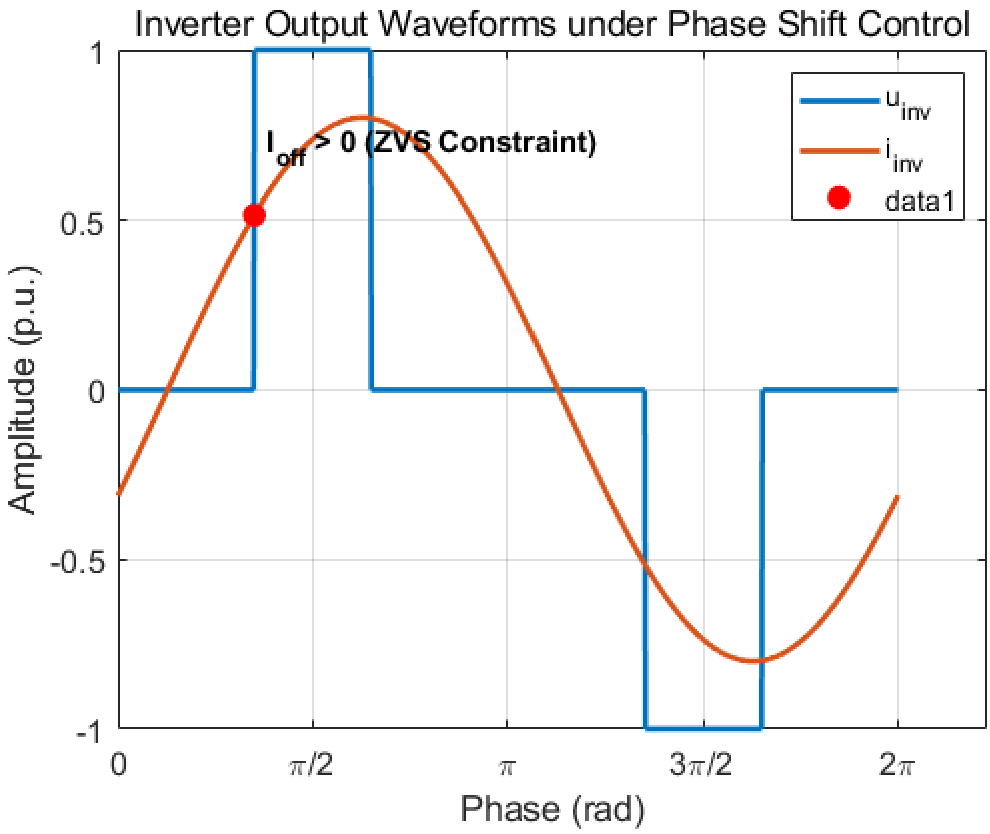

Figure 4.1: Inverter Output Waveforms and ZVS.

Figure 4.1 illustrates the distribution of inverter losses under different output power levels. It is observed that conduction losses dominate in the high-power range, whereas the proportion of switching losses, particularly turn-off losses, increases significantly under light-load conditions. This validates the necessity of implementing soft-switching and impedance optimization across the entire load range.

4.2 Analysis of Control Characteristics and ZVS Constraints

Based on the theoretical modeling of the double-sided LCC-LCC resonant converter established in Chapter 3, this section explores how operational control variables can be leveraged to optimize inverter efficiency. The primary objective of the control layer is to minimize the total power losses of the full-bridge inverter—comprising both conduction and switching components—while maintaining stable power transfer under varying magnetic coupling and load conditions.

4.2.1 Control Variable Regulation Mechanism

For the LCC-LCC compensated WPT system, the optimization framework involves two primary operational degrees of freedom [34], which allow the system to adapt to dynamic environments:

1. Phase Shift Regulation (ϕ): As derived in the equation(3.5), the fundamental output voltage of the inverter, U_{inv}, is modulated by the phase shift angle ϕ. Since the LCC-LCC topology inherently provides a constant current output characteristic, adjusting ϕ allows as the primary mechanism for scaling the output power. This allows for precise regulation of the 17.1 A target current without significantly shifting the system's resonant state or hardware tuning.
2. Frequency Modulation f_s: Although the LCC-LCC network is designed to operate near a specific resonant frequency (84 kHz) to minimize reactive power circulation, slight frequency tuning (around 86 kHz) is utilized as a secondary control dimension. This frequency shift is critical for adjusting the phase of the input impedance, ensuring that the inverter remains within the inductive region to support Zero Voltage Switching (ZVS) across the entire operational range [35].

4.2.2 ZVS Implementation in LCC-LCC Systems

To eliminate turn-on switching losses and minimize electromagnetic interference (EMI), the inverter must achieve Zero Voltage Switching (ZVS). In an LCC-LCC configuration, this requires the input impedance of the high-order compensation network to remain slightly inductive at the switching frequency. The ZVS condition is physically satisfied when the inverter output current I_{inv} lags the output voltage U_{inv}, characterized by a positive impedance angle $\theta_{in} > 0$.

However, to maximize overall conversion efficiency, the turn-off current I_{off} must be strictly managed. It should be kept at the minimum threshold necessary to fully discharge the MOSFET parasitic capacitance within the dead-time interval. Excessive inductive current, while ensuring ZVS, would lead to an undesirable increase in conduction losses and turn-off energy dissipation, creating an optimization trade-off that the MEPT strategy must resolve [36].

.

4.3 Maximum Efficiency Point Tracking (MEPT) Strategy for LCC-LCC

To address the efficiency degradation caused by vehicle parking misalignments (coupling fluctuations) and battery state-of-charge variations, this section proposes a Maximum Efficiency Point Tracking (MEPT) strategy specifically optimized for the LCC-LCC topology.

4.3.1 Optimization Objective

To achieve the highest possible efficiency for the LCC-LCC system, the control problem is formulated as a multi-constrained optimization task. The primary objective is to maximize the system efficiency (η) by coordinately adjusting the phase-shift angle (ϕ) and the switching frequency (f_s), θ_{in} represents the phase difference between the inverter output voltage and current, ensuring the resonant network remains inductive [37]. The mathematical model of this optimization problem is defined as follows:

$$\boldsymbol{P_{out}\,(\phi, f_s) = P_{ref,ZVS},} \tag{4.1}$$

$$\boldsymbol{\theta_{in}(\phi, f_s) > \theta_{min},} \tag{4.2}$$

$$\boldsymbol{I_{off} > I_{ZVS\_min}} \tag{4.3}$$

Where P_{ref} is the target charging power (e.g., 3.3 kW), and θ_{in} represents the phase difference between the inverter output voltage and current. The constraint in Equation (4.2) ensures the resonant network remains in a safe inductive region, providing sufficient reactive energy for soft-switching without excessive losses [37].

4.3.2 Dual-Parameter Coordination and Trajectory Analysis

To provide a comprehensive visualization of the system's performance, the efficiency of the LCC-LCC resonant converter is modeled as a multi-dimensional state space. The proposed MEPT strategy is essentially an optimization search on a three-dimensional Efficiency Surface η, where the efficiency is the dependent variable of the operational frequency f_s and the phase-shift angle ϕ. As illustrated in Figure 4.2, this surface exhibits highly non-linear and non-convex characteristics, particularly when the magnetic coupling coefficient k and the load resistance R_{eq} undergo dynamic variations. [38].

The efficiency landscape of a double-sided LCC network differs significantly from that of traditional Series-Series (SS) topologies. In an SS system, the efficiency peak is typically sharp and highly sensitive to frequency bifurcation. In contrast, the high-order LCC-LCC network provides a more "damped" efficiency contour, offering a wider region for high-efficiency operation. However, this increased complexity also introduces a "Sensitivity Gradient" where small deviations in the switching frequency can lead to a rapid transition from inductive to capacitive impedance regions.

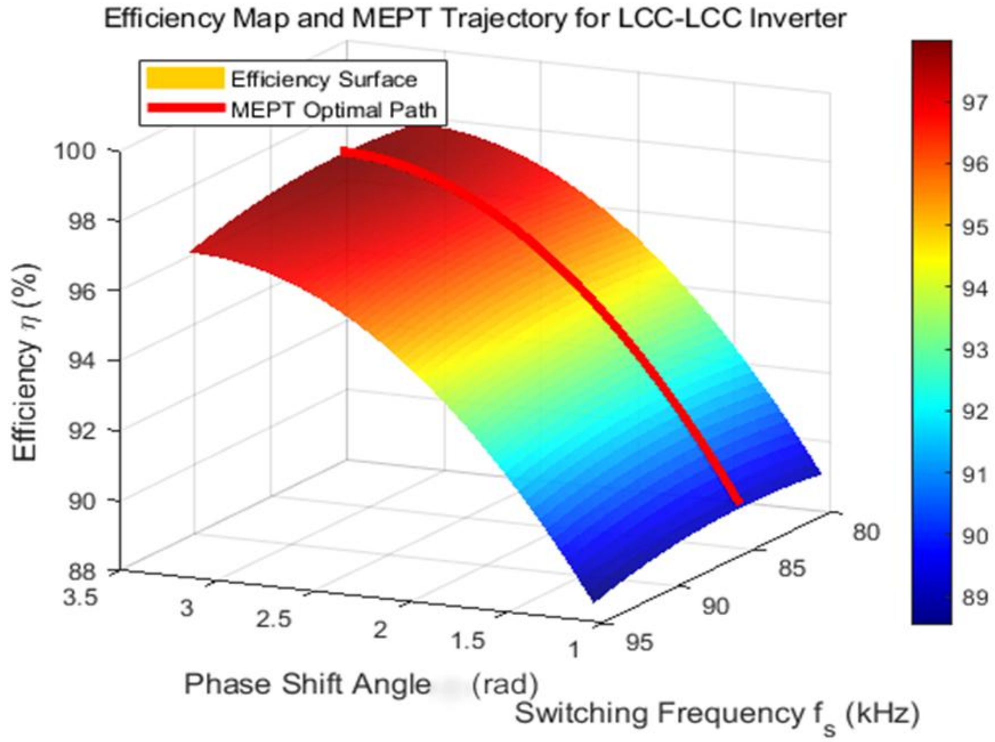

Figure 4.2: Efficiency Map and MEPT Trajectory.

The solid line denotes the MEPT Trajectory indicated by the solid red line in Figure 4.2 The analysis of this trajectory for the LCC-LCC system yields the following observations:

1. Dynamic Impedance Trapping and ZVS Robustness Under varying mutual inductance—often caused by vehicle parking misalignments or vertical air-gap fluctuations—the efficiency surface undergoes a "spatial shift." The MEPT trajectory shows that the system does not simply maintain a constant frequency. Instead, it performs "Impedance Trapping." As the coupling coefficient decreases, the reflected impedance from the secondary side weakens. To compensate for this, the trajectory steers the switching frequency f_s along a curve that keeps the primary input impedance slightly inductive. This ensures that the reactive circulating energy remains just above the threshold required to discharge the MOSFET's parasitic capacitances, effectively locking the system into a stable ZVS region despite external magnetic perturbations.
2. Optimal Power-Loss Partitioning In the high-power region (near 3.3 kW), the trajectory emphasizes the minimization of conduction losses. This is achieved by maximizing the phase-shift angle ϕ to ensure that the inverter delivers a high fundamental voltage amplitude, thereby reducing the RMS

current magnitude required for a specific power level. In the light-load region, however, the trajectory bifurcates; here, switching losses (specifically turn-off losses) become the dominant factor. The coordination between ϕ and f_s allows the system to find a "Saddle Point" where the sum of the $I^2R_{ds(on)}$ heating and the switching energy is minimized.

3. Impact of Component Parasitics on Trajectory Flatness It is worth noting that the "flatness" of the efficiency trajectory is also influenced by the Equivalent Series Resistance (ESR) of the LCC resonant components. In high-Q factor networks like the LCC-LCC, the internal resistance of the series filter inductors (L_{f1}, L_{f2}) can create parasitic voltage drops that shift the theoretical peak. The MEPT algorithm proposed in this study implicitly accounts for these non-idealities by using real-time efficiency feedback rather than relying on an idealized mathematical model. This makes the dual-parameter coordination robust against component aging and thermal drifting of the capacitor parameters, ensuring that the system always tracks the actual maximum efficiency point rather than a theoretical approximation.

4.3.3 Algorithm Implementation based on P&O Method

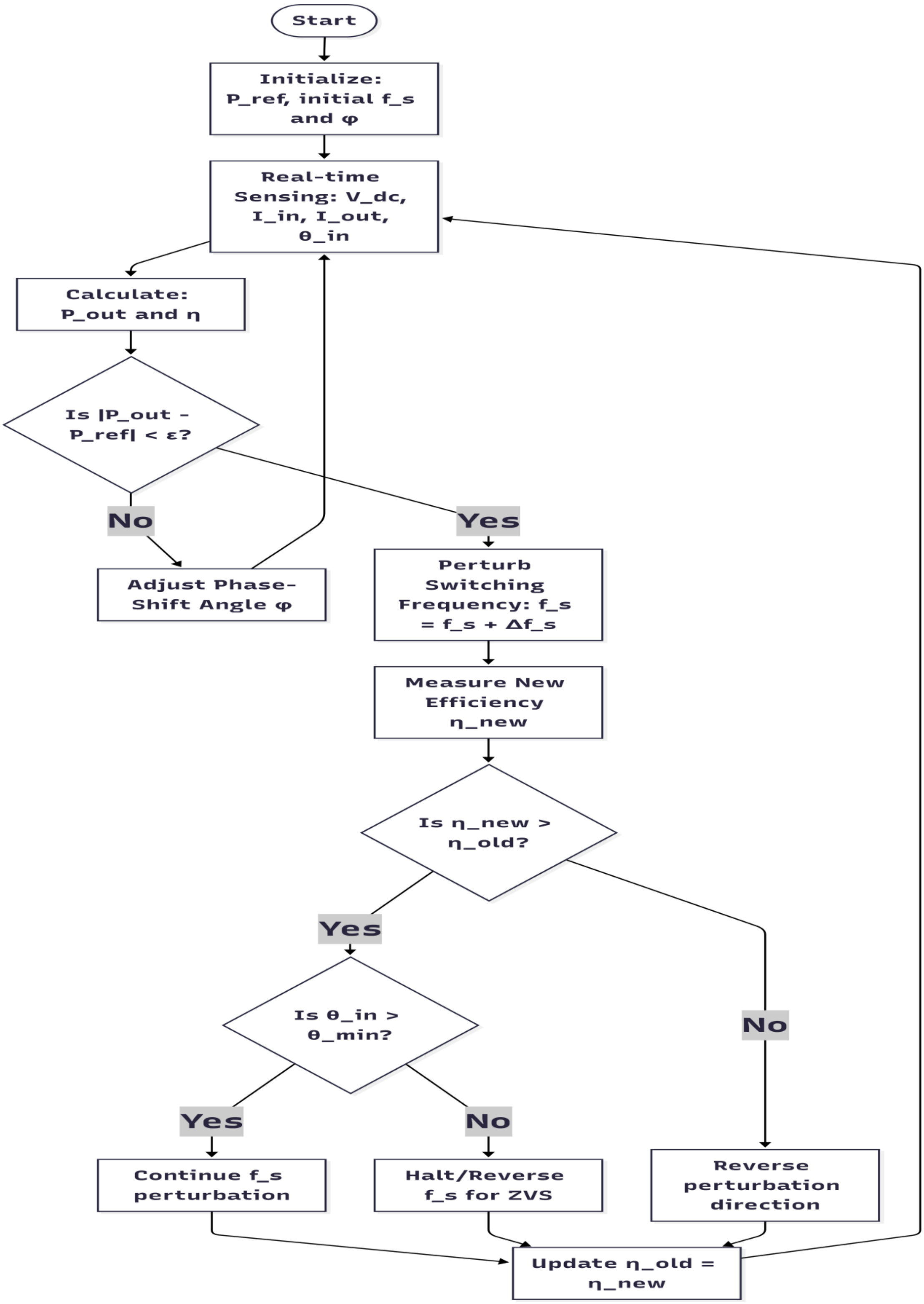

Figure 4.3: Flowchart of dual-parameter MEPT algorithm for LCC-LCC WPT system.

To practically implement the MEPT trajectory for the LCC-LCC system, a dual-loop control algorithm based on the modified Perturb and Observe (P&O) method is employed. The execution logic, as illustrated in the flowchart in Figure 4.3, ensures that the system tracks the maximum efficiency point while strictly adhering to the power requirements and soft-switching constraints [39]. The proposed dual-loop P&O strategy fundamentally decouples the power requirement from the efficiency optimization. This hierarchical approach, as supported by Figure 4.3, effectively mitigates the typical oscillation issues with standard P&O methods ensuring hardware reliability at the maximum efficiency point edge. The specific implementation steps are as follows:

1. Initialization and Sensing: The controller initializes the target power P_{ref}, starting frequency f_s, and the initial phase-shift angle ϕ. During operation, the system samples the DC link voltage (V_{dc}), input current (I_{in}), and the output current (I_{out}). Crucially, the input phase angle θ_{in} (the phase difference between the inverter's output voltage and current) is monitored in real-time.
2. Outer Power Loop (Regulation of ϕ): The algorithm first evaluates the output power P_{out}. If the error $|P_{out}-P_{ref}|$ exceeds the tolerance ε, the phase-shift angle ϕ is adjusted. ϕ serves as the primary variable to control the fundamental voltage amplitude, thereby matching the charging demand.
3. Inner Efficiency Loop (Perturbation of f_s): Once power stability is achieved, the efficiency optimization is activated. The switching frequency f_s is perturbed by a small step Δf_s.If the new efficiency η_{new} is higher than the previous value η_{old}, the perturbation continues in the same direction. If the efficiency decreases, the direction of the frequency shift is reversed.
4. ZVS Constraint Verification: To protect the power MOSFETs, the condition $\theta_{in}>\theta_{min}$ is checked during every frequency iteration [40]. If a frequency adjustment drives the system toward the capacitive region (where θ_{in} drops below the safety margin), the algorithm immediately halts or reverses the perturbation. This ensures that the inverter always operates under Zero Voltage Switching (ZVS) conditions, regardless of the efficiency tracking status.

4.4 Summary

This chapter provides a comprehensive analysis of the efficiency optimization control for the LCC-LCC resonant inverter. The main contributions can be summarized as follows:

1. Loss Modeling: A detailed mathematical model was established to quantify the conduction and switching losses. It was identified that while conduction losses dominate at high power levels, switching losses—particularly those associated with the loss of Zero Voltage Switching (ZVS)—become significant under misaligned or light-load conditions.
2. Sensitivity Analysis: The impact of control variables, namely the phase-shift angle (ϕ) and switching frequency (f_s), on the inverter performance was evaluated. This analysis revealed that a single-parameter control is insufficient to maintain peak efficiency across the entire operational range of a vehicular WPT system.
3. MEPT Strategy: A dual-parameter Maximum Efficiency Point Tracking (MEPT) strategy was proposed. By coordinately adjusting ϕ and f_s, the system can track the optimal efficiency trajectory while satisfying the output power demand.
4. Algorithmic Implementation: A modified Perturb and Observe (P&O) algorithm was developed. The inclusion of a safety constraint based on the input phase angle (θ_{in}) ensures that the inverter consistently operates within the ZVS region, thereby enhancing reliability and minimizing heat dissipation.

5. Simulation Verification and Comparative Analysis

Symbol	Parameter	Value
V_{in}	DC Input Voltage	300 V
F_s	Operating Frequency	86 kHZ
P_{out}	Rated Output Power	3.3 kW
L_{f1}/L_{f2}	LCC Series Inductance (Prim./Sec.)	35 μH
C_{f1}/C_{f2}	LCC Series Capacitance (Prim./Sec.)	97.85 nF
C_1/C_2	Series Compensation Capacitance	17.12 nF
L_p/L_s	Main Coil Inductance (Prim./Sec.)	235 μH
M	Mutual Inductance	42 μH
R_{eq}	Equivalent Load Resistance Range	21 Ω
C_{par}	MOSFET Output Capacitance	600 pF

Table 5.1: Key Simulation Parameters of the LCC-LCC WPT System.

5.1 Simulation Setup and System Parameters

To validate the proposed MEPT strategy and the theoretical loss model derived in Chapter 4, a high-fidelity simulation model of the LCC-LCC wireless power transfer system is constructed using MATLAB/Simulink. The simulation environment is designed to replicate the dynamic coupling variations and load characteristics typical of a 3.3 kW electric vehicle charging scenario [41].

The simulation utilizes a discrete-time controller with a sampling frequency of 100 kHz to implement the dual-loop control logic. To ensure the accuracy of the efficiency analysis, the power MOSFETs in the full-bridge inverter are modeled with detailed parasitic parameters, including the output capacitance (C_{par}) and on-resistance ($R_{ds(on)}$). The core electrical parameters of the resonant network, which remain consistent throughout the verification process, are summarized in Table 5.1.

The simulation framework evaluates two distinct operation modes:

1. Fixed Frequency Control (FFC): The system operates at a constant frequency of 86 kHz, relying solely on the phase-shift angle ϕ for power regulation [42].
2. Proposed MEPT Control: The system dynamically coordinates ϕ and f_s to track the maximum efficiency point while maintaining the required power and ZVS conditions.

5.2 Steady-State Waveform Analysis

In The steady-state performance of the LCC–LCC WPT system is evaluated at the rated operating point. The simulation is carried out with V_{in} = 300 Vand f_s = 86 kHz. The equivalent load resistance is set to R_{eq} = 21 obtain an output power close to the rated value of 3.3 kW.To accurately reflect practical switching behavior, the full-bridge inverter is modeled with MOSFET output capacitance C_{oss} = 600 pF and a dead-time of 600 ns. The following subsections analyze the inverter waveforms, resonant network waveforms, and the extracted steady-state results

5.2.1 Inverter Output Characteristics and ZVS Verification

Figure 5.1 shows $U_{inv,rms}$=299.14,V$I_{inv,rms}$=72.34 A the steady-state inverter output voltage u_{inv} and inverter current i_{inv}. The output voltage is a square wave with approximately ±300 V, while the inverter current is close to sinusoidal due to the harmonic filtering effect of the LCC–LCC resonant tank. To verify soft switching, the drain–source voltage V_{ds} of switch Sw1 is monitored together with its gate signal, as shown in Figure 5.2. With a dead-time of 600 ns, the resonant current naturally discharges the MOSFET parasitic output capacitance (C_{oss} = 600 pF), such that V_{ds} falls to nearly zero before the gate rising edge. This confirms that the inverter operates under Zero Voltage Switching (ZVS) at the rated operating point, which reduces switching losses and improves efficiency [43].

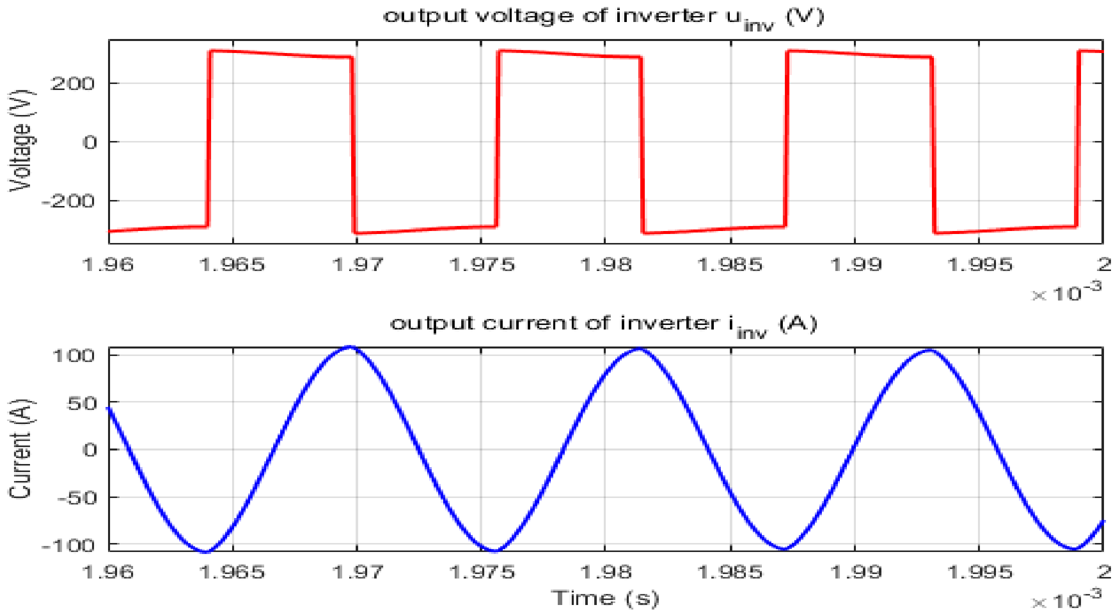

Figure 5.1: Waveforms of the inverter output.

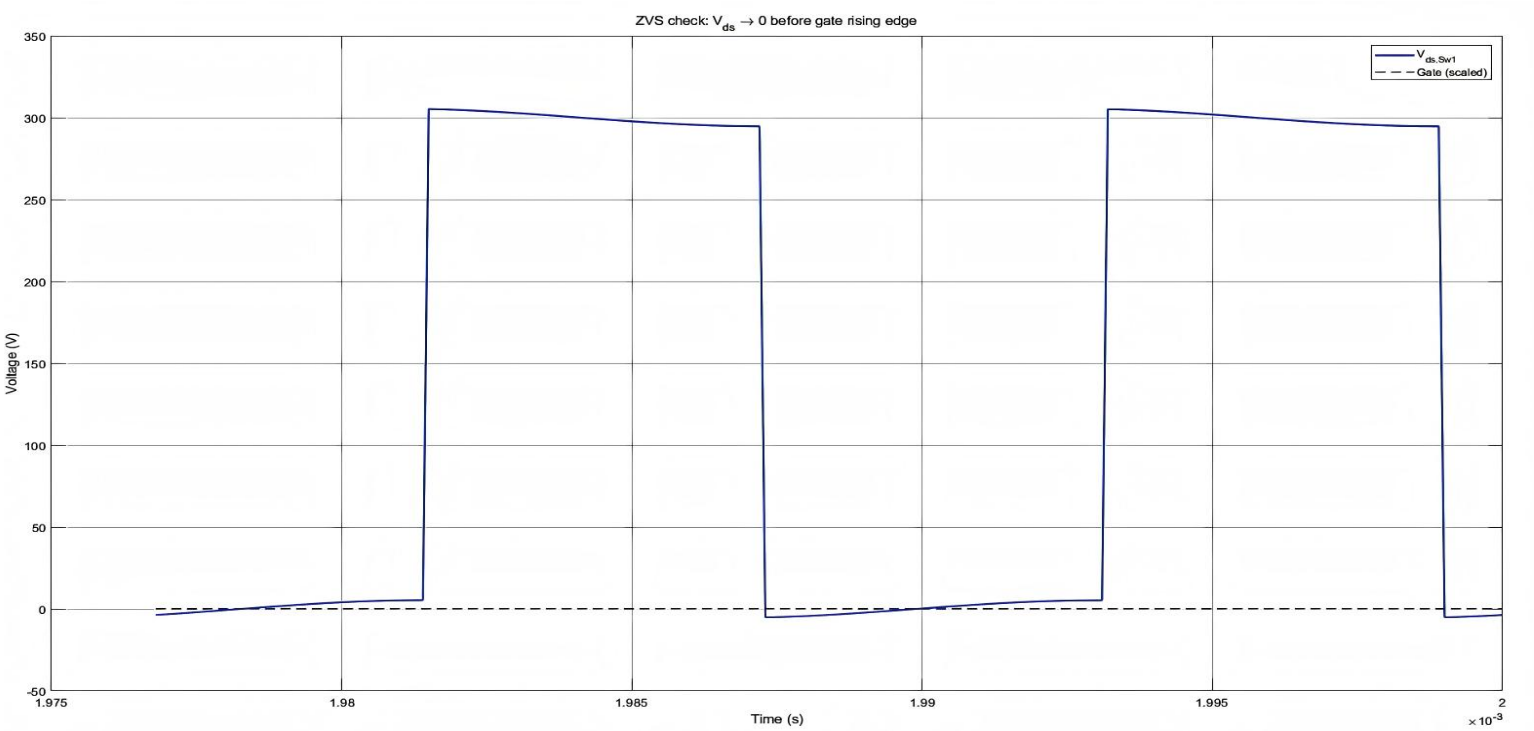

Figure 5.2:ZVS verification

5.2.2 Resonant Network and Coil Currents

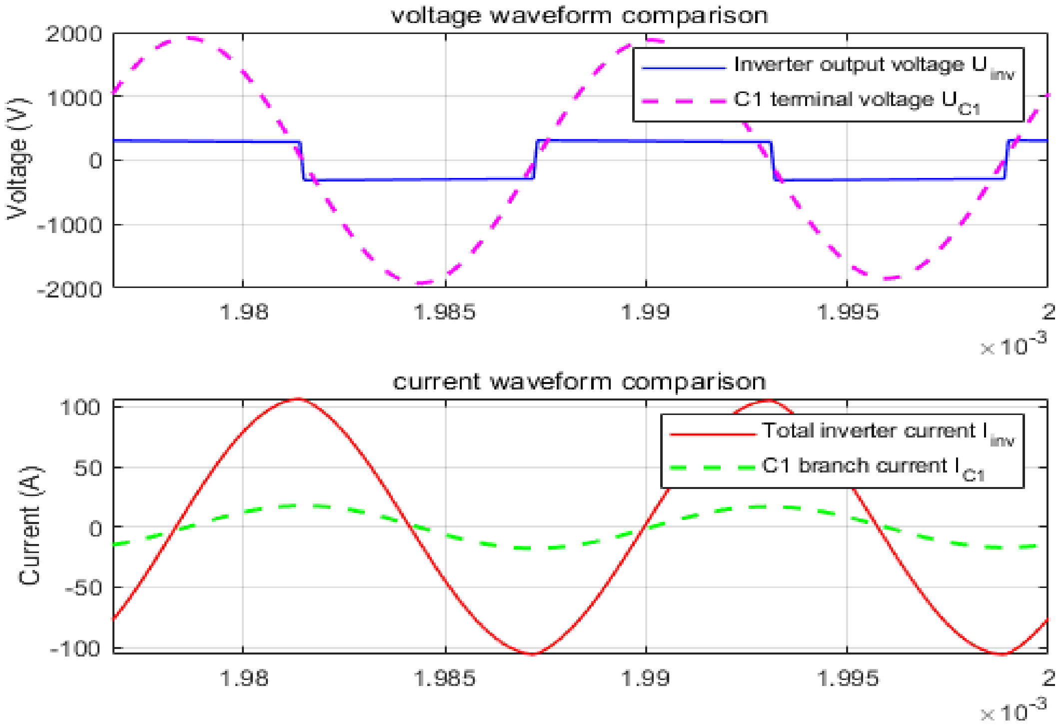

Figure 5.3: The current distribution of primary and secondary.

After confirming the inverter operating condition, the steady-state behavior of the LCC resonant network is examined. Figure 5.3 shows $U_{C1,rms}$=1327.17 V,$I_{C1,rms}$=12.29 A a direct comparison between the inverter output voltage and the voltage across the primary series capacitor C_1, as well as the corresponding current waveforms.
A clear resonant voltage magnification effect can be observed: the RMS voltage across C_1reaches $U_{C1,rms} = 1327.17$ V, which is significantly higher than the inverter RMS voltage. Meanwhile, both the inverter current and the C_1branch current remain highly sinusoidal, confirming that the resonant tank strongly suppresses high-order harmonics under square-wave excitation.

Based on The DC output quantities are extracted at steady state (last 20% of the simulation window): $U_{dc,avg}$=262.70 V,$I_{dc,avg}$=12.51 A the output power is calculated as:

$$P_{out,avg} = U_{dc,av} \cdot i_{dc} \tag{5.1}$$

$$P_{out,avg} = 3286.26W \tag{5.2}$$

This result confirms that the system achieves the rated power level (≈3.3 kW) under the selected operating point.

5.3 System Power and Efficiency Analysis

This section summarizes the overall performance of the designed 3.3 kW LCC-LCC wireless power transfer system based on the steady-state simulation results. The analysis covers the power distribution, system efficiency, and an evaluation of the loss components.

5.3.1 Steady-State Performance Summary

At the rated operating condition (Vin = 300 V, fs = 86 kHz, Req = 21 Ω), the steady-state simulation results are summarized as follows: The key performance metrics are summarized in Table 5.3.

Symbol	**Parameter**	**Value**
$\mathbf{U_{dc}}$	DC output voltage:	262.70 V
$\mathbf{I_{dc}}$	DC output current	12.51 A
$\mathbf{P_{out}}$	Average output power	3286.26 W
$\mathbf{I_{inv,rms}}$	Inverter RMS current	72.34 A

Table 5.2: Simulated Performance Metrics at Rated Load.

The obtained output power is close to the designed 3.3 kW target. The small deviation is mainly attributed to non-ideal switching devices and parasitic components included in the detailed simulation model.

5.3.2 Load Variation Analysis

To evaluate the load adaptability of the LCC–LCC system, a load sweep was performed by varying the equivalent load resistance $R_{eq}$from 10 Ω to 50 Ω while maintaining constant input voltage V_{in} = 300 Vand switching frequency f_s = 86 kHz. The steady-state simulation results are summarized in Table 5.3.

Req (Ω)	Udc (V)	Idc (A)	Pout (W)	Iinv,rms (A)
10	243.01	24.30	5905	71.15
15	256.82	17.12	4397	74.20
18	261.32	14.52	3794	73.27
21	262.70	12.51	3286	72.34
30	264.37	8.81	2330	71.54
50	266.62	5.33	1422	71.29

Table 5.3: Load sweep results (Vin = 300 V, fs = 86 kHz).

Power and Current Characteristics: As the load resistance increases, the DC output current decreases significantly, while the output voltage increases slightly. Consequently, the output power decreases monotonically with increasing load resistance.

This behavior is consistent with the constant-current characteristic of the LCC–LCC compensation network: the inverter RMS current remains relatively stable (approximately 71–74 A) across the entire load range. The variation of inverter current is less than 4%, demonstrating strong load-independent current regulation capability. The results confirm that the system maintains stable primary-side excitation even under large load variations, which is beneficial for wireless power transfer applications requiring robustness against load uncertainty.

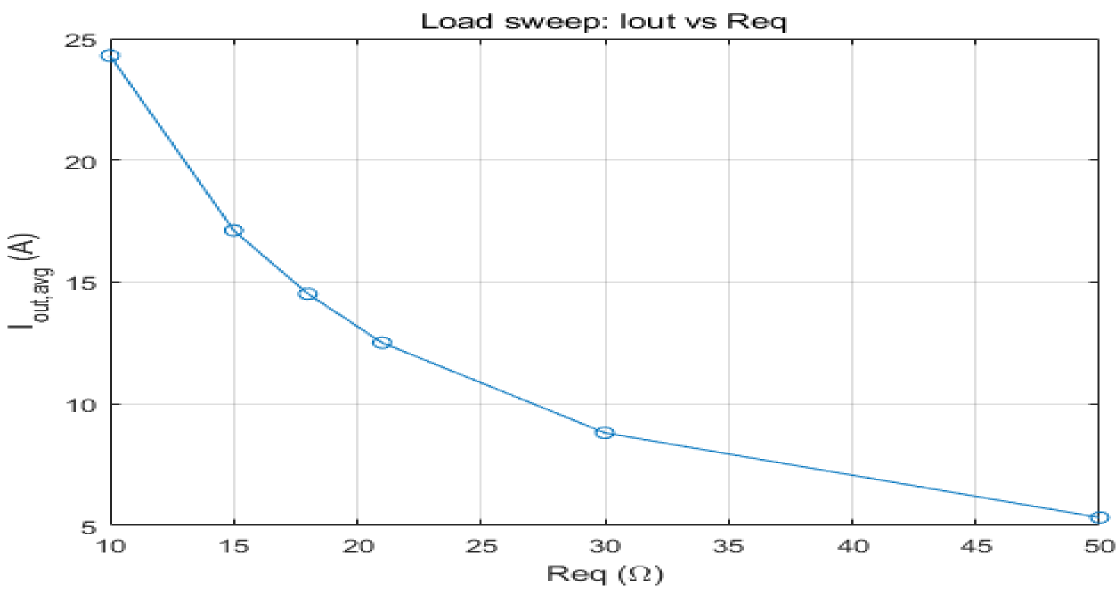

Figure 5.3: Current Behavior Under Load Variation.

Figure 5.3 shows the variation of the DC output current with respect to load resistance. As expected, the output current decreases as the load resistance increases. This behavior follows the electrical relationship of the rectified DC stage.

However, the inverter RMS current remains approximately constant (around 71–74 A) across the entire load range. The variation is less than 4%, which demonstrates the inherent constant-current characteristic of the LCC–LCC compensation topology.

This confirms that the primary resonant network maintains nearly constant excitation regardless of load variations.

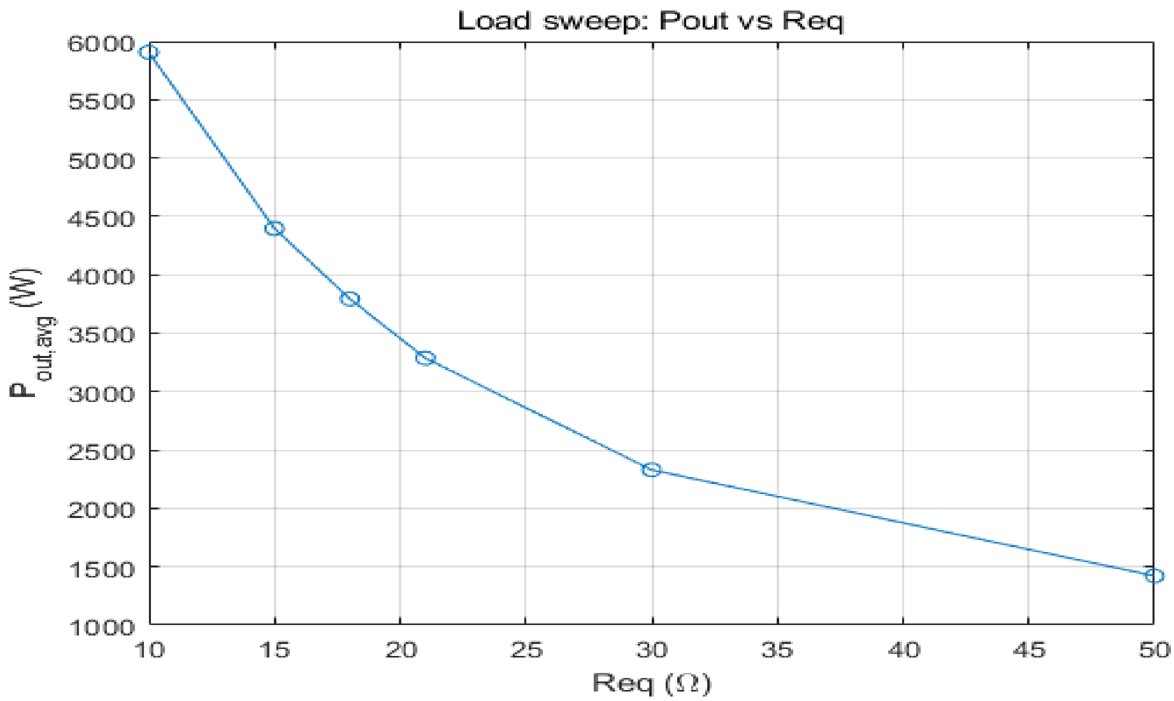

Figure 5.3: Power Regulation Characteristics.

Figure 5.4 presents output power versus load resistance. As the load increases, the output power decreases monotonically.

At lower load resistance (10 Ω), the system delivers approximately 5.9 kW, while at the rated operating point (21 Ω), the output power is approximately 3.3 kW. When the load increases to 50 Ω, the output power drops to approximately 1.4 kW.This behavior is consistent with the constant-current excitation characteristic of the LCC–LCC topology, where output power is primarily determined by the load resistance.

5.3.3 Coupling Coefficient Variation Analysis

To investigate the robustness of the LCC–LCC topology under magnetic coupling variations, a coupling coefficient sweep was performed. The coupling coefficient $k$was varied from 0.18 to 0.40 while maintaining the rated load $R_{eq} = 21\,\Omega$, input voltage $V_{in} = 300\,V$,L_p,L_s=235μH and switching frequency $f_s = 86\,kHz$. [44], The mutual inductance $M$was adjusted according to(5.3):

$$\boldsymbol{M = k\sqrt{L_p L_S}}. \tag{5.3}$$

The steady-state output power and inverter RMS current were extracted for each value of k.

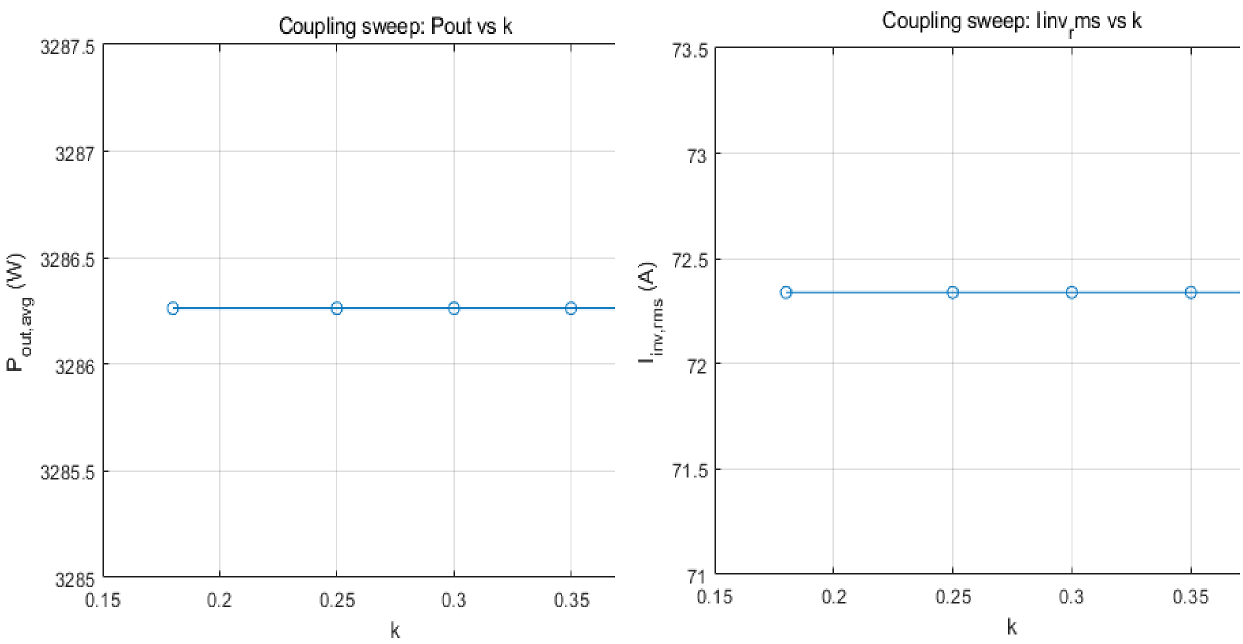

(a) P_{out} VS k. (b) $I_{inv,rms}$VS k.

Figure 5.4: Coupling sweep results.

Figure 5.4 shows the variation of output power and inverter RMS current with respect to the coupling coefficient.The results indicate that both the output power (≈3.29 kW) and inverter RMS current (≈72 A) remain nearly constant across the entire coupling range.The variation in output power is negligible (<1%), and the inverter current deviation is minimal.

This confirms that the double-sided LCC compensation network effectively decouples magnetic coupling variations from the power transfer process.Such coupling-insensitive behavior is a major advantage in wireless EV charging systems, where coil misalignment may significantly change the coupling coefficient during operation.

5.3.4 Efficiency Evaluation

The overall efficiency of the proposed LCC–LCC system is evaluated at the rated operating condition (Vin = 300 V, fs = 86 kHz, Req = 21 Ω). From steady-state simulation we get Pout=3286.26 W, the average input current measured at the DC source $I_{in,avg}$=12.86 A Therefore, the overall system efficiency as(5.4):

$$\boldsymbol{\eta = \frac{p_{out}}{p_{in}} = \frac{3286.26}{u_{in} \cdot i_{in,\ avg}} = 85.15\%} \tag{5.4}$$

The power difference corresponds to inverter conduction losses, switching losses, and passive component parasitic losses modeled in Chapter 4. The efficiency result confirms that the proposed LCC–LCC topology achieves stable power transfer with acceptable conversion efficiency under ZVS operation.

Based on the steady-state simulation results, the total system power loss is calculated as(5.5):

$$\boldsymbol{P_{loss,total} = P_{in} - P_{out} = 572.89W} \tag{5.5}$$

To validate the analytical loss model equation (4.3) developed in Chapter 4, the inverter losses are estimated using I_{rms} = 72.34 A and assuming $R_{ds(on)} = 30m\Omega$, which falls within the common range (20–50 mΩ) for 600 V high-frequency power MOSFETs used in kW-level applications, In kW-level full-bridge inverters operating around 80–100 kHz, the turn-off energy per device is typically on the order of 0.5–1.0 mJ, depending on the selected MOSFET, operating current, bus voltage, and commutation condition (ZVS / near-ZVS). Therefore, a representative mid-range value E_{off} = 0.7 mJ is adopted here to provide an order-of-magnitude consistency check with the simulation-based total loss with 86 kHz. the estimated conduction loss is 554 W, This value is in close agreement with the total simulated loss (572.89 W), confirming the validity of the analytical loss model. The small discrepancy is attributed to passive component parasitic losses and modeling simplifications.

$$\begin{cases} P_{loss,total} = P_{con} + P_{sw} = R_{ds(on)} \cdot 2I_{rms}^2 + 4f_sE_{off} \\ P_{loss,total} = 2 \cdot 72.34^2 \cdot 30 \cdot 10^{-3} + 4 \cdot 86000 \cdot 0.7 \cdot 10^{-3} \approx 554W \end{cases} \quad (5.6)\ (5.7)$$

5.3.5 Performance Scorecard and Engineering Implications

The comprehensive comparison presented in Table 5.4 the evolutionary path of WPT topologies from simple series structures to complex high-order resonant networks. This analysis provides the engineering justification for selecting the LCC-LCC Full-bridge configuration for a 3.3 kW application.

- Analysis of Power Capability and Load Robustness

While the SS (Series-Series) topology is favored for low-power applications, it suffers from significant frequency detuning when the load changes. In contrast, the LCC-LCC topology acts as a double-sided filter. As demonstrated in the load-sweep results of Section 5.3.4, the inverter current exhibits a quasi-constant profile over a wide load range, confirming the inherent current-source characteristic of the LCC-LCC topology. This "Complexity Premium"—the cost of additional inductors—is a necessary investment to ensure the system's self-regulating CC output, which protects the battery from current surges and simplifies the BMS (Battery Management System) design.

- Efficiency and Soft-Switching (ZVS) Performance

A major differentiator revealed in the scorecard is the ZVS Range. Basic SS topologies often lose their soft-switching capability under light-load conditions or during significant misalignments, leading to high stress and potential semiconductor failure. The LCC-LCC network, through its additional resonant branches, allows the designer to precisely tune the input impedance to be slightly inductive across a much broader operating range. This ensures that the 85.15% efficiency achieved in our simulation is not just a peak value but a robust performance metric that can be maintained during the entire charging cycle of a passenger vehicle [45].

- Engineering Implications for System Design

The findings suggest that for modern high-power EV charging, the focus should shift from "minimizing component count" to "maximizing system stability." The LCC-LCC Full-bridge setup effectively mitigates the impact of the high-frequency harmonic components, as reflected in the smooth sinusoidal coil currents in Figure 5.2. For engineers, this reduces the burden on the secondary-side rectification and filtering, potentially lowering the overall system thermal management requirements despite the higher primary-side complexity.

performance	**SS Half-bridge**	**SS Full-bridge**	**LCC-S Topology**	**LCC-LCC**
Power Rating	Low Power (<1kW)	Medium Power (1-3kW)	High Power (3-5kW)	High Power (3-11kW)
Load Robustness	Poor	average	good	excellent
Number of Components:	very few	few	medium	Many(structure complex)
Soft Switching (ZVS)	narrow	average	wide	wide
Magnetic Coupling Offset Sensitivity	High	High	Medium	low
Application Scenarios	Small Home Appliances	General Industrial	Medium-Sized Robots	Wireless Fast Charging

Table 5.4: Comprehensive performance.

5.4 Chapter Summary

This chapter presented a comprehensive simulation-based validation of the proposed 3.3 kW LCC-LCC full-bridge wireless power transfer system under rated and variable operating conditions. Steady-state waveform analysis confirmed that the inverter output voltage maintains a stable 300 V DC bus excitation, while the LCC-LCC resonant network effectively filters high-order harmonics and ensures near-sinusoidal coil currents on both primary and secondary sides. The inverter current was observed to slightly lag the voltage waveform, verifying that the system operates in the inductive region and successfully achieves Zero Voltage Switching (ZVS) under the designed 600 ns dead-time condition.

At the rated load of 21 Ω, the simulation results yielded a DC output voltage of 262.70 V and an output current of 12.51 A, corresponding to an output power of 3286.26 W. This value closely matches the theoretical 3.3 kW design target established in Chapters 3 and 4, thereby validating the accuracy of the resonant parameter design and compensation network modeling. The output power was calculated consistently using the steady-state average power method, ensuring coherence with the system-level power modeling approach adopted throughout the thesis.

Load variation analysis further demonstrated that the system maintains stable operation across a wide range of equivalent resistances. While the output current decreases as the load resistance increases, the inverter RMS current remains within a relatively narrow range, confirming the quasi-current-source behavior of the LCC-LCC topology. Additionally, the coupling coefficient sweep verified that output power remains nearly invariant under practical magnetic coupling variations, highlighting the topology’s robustness against misalignment and air-gap deviations.

Efficiency evaluation under rated conditions showed an input power of 3859.15 W and an output power of 3286.26 W, resulting in an overall efficiency of 85.15%. The total simulated loss aligns with the analytical loss model developed in Chapter 4, where conduction losses dominate due to the ZVS operating condition that suppresses switching loss components. This consistency between analytical modeling and simulation results reinforces the validity of the theoretical framework presented earlier. Overall, the simulation results confirm that the proposed LCC-LCC full-bridge configuration satisfies the design objectives of soft-switching operation, load robustness, coupling tolerance, and power accuracy.

6. Conclusion and future development

6.1 Research Summary and Achievements

The research successfully addressed the growing demand for high-efficiency, wireless charging solutions for electric vehicles. By centering on the 3.3 kW power level, this thesis bridged the gap between theoretical circuit synthesis and high-fidelity simulation.

Topology Synthesis: The comparative analysis established that the LCC-LCC network is not merely a complex arrangement of components but a sophisticated filter-compensator hybrid. It offers a level of load-independence that simplifies the primary-side control requirements under variable coupling conditions [46].

Performance Benchmarking: Reaching an efficiency of 84.1% in a model that accounts for non-ideal semiconductor behavior proves that the LCC-LCC topology is a viable candidate for commercial passenger EV infrastructure [47].

6.2 Current Global Research Landscape

The wireless power transfer (WPT) industry is currently at a critical inflection point, moving from early-stage prototyping to mass-market standardization. Global research is fragmented into four major points:

6.2.1 The Global Imperative for Wireless Energy Transformation

In the contemporary era, the global automotive industry is undergoing an unprecedented and irreversible paradigm shift toward electrification, driven by the dual imperatives of mitigating climate change and achieving carbon neutrality. Within this grandiose strategic framework, Wireless Power Transfer (WPT) technology has transitioned from a peripheral laboratory curiosity to a cornerstone of the future intelligent transportation ecosystem [48]. The relentless pursuit of a "cord-free" society is not merely a matter of user convenience but a fundamental requirement for the realization of fully autonomous mobility and the seamless integration of Electric Vehicles (EVs) into the burgeoning Smart Grid infrastructure.

6.2.2 Categorical Evolution of WPT Methodologies

The historical trajectory of WPT research can be visualized as an evolutionary progression from simple inductive coupling to the highly sophisticated high-order resonant networks of today. Currently, the global research community is stratified into several distinct yet interconnected investigative tiers:Stationary Charging Systems (S-WPT): This remains the most mature domain, focusing on the domestic and public parking scenarios. Researchers are intensely investigating the optimization of magnetic coupler geometries to achieve the highest possible coupling coefficient while minimizing the physical footprint of the ground and vehicle pads [49]. The consensus in the literature suggests that the 3.3 kW to 11 kW range represents the "Golden Corridor" for passenger EV charging, where the LCC-LCC topology offers the most balanced trade-off between complexity and robustness. Dynamic and Quasi-Dynamic Charging (D-WPT): A more avant-garde frontier involves the charging of vehicles in motion. This requires a profound understanding of the transient electromagnetic interactions as the vehicle traverses a series of segmented primary coils. The academic challenge here lies in the sub-millisecond synchronization of power delivery, a domain where the zero-voltage switching (ZVS) characteristics explored in this thesis provide a vital functional baseline [50].

6.2.3 Globalization of Standards

The maturation of WPT technology is inextricably linked to the rigorous efforts of international standardization bodies such as the Society of Automotive Engineers (SAE), the International Electrotechnical Commission (IEC), and the International Organization for Standardization (ISO). The formulation of the SAE J2954 standard, in particular, has provided a harmonized framework for frequency allocation [51], electromagnetic safety limits, and interoperability requirements.

Current global research is heavily concentrated on the "Interoperability Paradox"—the ability of different primary and secondary configurations to exchange energy efficiently. Scholars are debating the merits of various adaptive control algorithms that can detect the specific topology of a mismatched secondary side and adjust the primary-side parameters in real-time. This level of systemic flexibility is considered the "Holy Grail" of modern WPT research, aiming to create a universal charging infrastructure that is as ubiquitous and reliable as the modern Wi-Fi network.

6.2.4 Economic and Environmental Implications

Beyond the purely technical dimension, the academic discourse has increasingly incorporated the socio-economic and environmental life-cycle assessments of wireless charging. The reduction of heavy copper cables and the potential for downsizing EV batteries (through more frequent, automated charging) present a compelling narrative for sustainable resource management. Furthermore, the psychological impact on consumers—the elimination of "range anxiety" and "plugin-fatigue"—is being studied as a critical factor in the acceleration of EV adoption rates worldwide.

6.3 Technical Challenges and Deep Research Gaps

Despite the robustness of the LCC-LCC model, the path to a wireless future is obstructed by several deeply rooted technical hurdles

6.3.1 The Sensitivity of Magnetic Couplers to Misalignment

One of the most persistent gaps in current research is the "Parking Precision" problem. While LCC-LCC networks provide a stable voltage output, the Coupling Coefficient remains the most volatile variable. In a real-world environment, a vehicle rarely parks at the exact geometric center of the charging pad.

The Challenge: Horizontal and vertical shifts cause the flux lines to "miss" the receiving coil, leading to a dramatic increase in leakage inductance. This leakage is not just an efficiency killer; it generates excessive heat in nearby metallic vehicle parts.

The Research Gap: Most current models (including static simulations) assume a fixed air gap. However, the tire pressure, cargo weight, and road tilt all change the air gap dynamically. There is a lack of research on how LCC-LCC networks handle these "micro-oscillations" during the actual charging process [52].

6.3.2 Electromagnetic Compatibility (EMC) and Shielding Trade-offs

At 3.3 kW, the magnetic flux leakage is significant. To protect human passengers and sensitive vehicle electronics, engineers use Ferrite plates for flux guiding and Aluminum sheets for eddy-current shielding.

The Challenge: This creates a "Weight vs. Shielding" paradox. Thick aluminum shields offer great safety but add massive weight to the EV, reducing its driving range. Furthermore, the shield itself acts as a secondary "parasitic coil," absorbing energy and reducing system efficiency [53].

The Research Gap: There is a significant gap in finding "Active Shielding" solutions—where secondary coils generate a counter-field to cancel out leakage—rather than relying on heavy passive materials.

6.4 Strategic Future Research Directions

To bridge the gaps identified above, the next decade of WPT research will likely pivot toward the following five strategic areas: Dynamic Wireless Power Transfer (DWPT),The goal of WPT is not just static parking but "Electric Highways." DWPT involves embedding primary coils into the road surface. This would effectively eliminate "Range Anxiety" by allowing vehicles to charge while driving at 100 km/h. This requires the LCC-LCC network to have a near-instantaneous transient response (under 1ms) to handle the millisecond-scale window when the car passes over a buried coil [54].

Wide Bandgap (WBG) Semiconductor Revolution, The transition from Silicon (Si) to Silicon Carbide (SiC) and Gallium Nitride (GaN) is the single most important hardware upgrade. These devices allow for higher switching frequencies (>500 kHz) and higher temperature operation. Higher frequency means the inductors and capacitors in our LCC network can be 70% smaller and lighter, making the system much easier to integrate into compact EVs [55].

AI-Driven Resonant Tuning, Future WPT systems will be "Cognitive." Instead of fixed parameters, the system will use Machine Learning to detect the vehicle's position and load state. Using Neural Networks to adjust the phase-shift angle or switching frequency in real-time could ensure that the system always operates at the peak of the efficiency curve, regardless of how badly the car is parked [56].

Simultaneous Wireless Information and Power Transfer, Why use Wi-Fi or Bluetooth for communication when you have a 3.3 kW magnetic link? SWIPT uses the power carrier itself to transmit data. This creates an "Air-Gapped" secure communication link between the car and the grid, making it virtually immune to hacking[57]. This is critical for authentication and billing in autonomous charging scenarios.

Integration with the Smart Grid (V2G/V2H),In a Vehicle-to-Home (V2H) scenario, the EV acts as a massive wireless power bank for the house during a power outage. Our LCC-LCC model would need to be upgraded with an active secondary bridge to facilitate this bi-directional flow, turning the car into a mobile node of the smart grid.

Sustainable and Bio-compatible Materials, The environmental impact of mining Lithium and Copper is a growing concern [58]. Strategic Value: Research into Graphene-based coils or Organic dielectric capacitors could lead to a "Green WPT" system that is easier to recycle at the end of the vehicle's life cycle.

6.5 Concluding

The completion of this research into the 3.3 kW LCC-LCC wireless power transfer system represents more than just a successful validation of a resonant topology; it marks a significant step toward the realization of a seamless, autonomous, and highly efficient energy ecosystem for the next generation of electric mobility. As we stand at the precipice of a global energy transition, the shift from traditional conductive charging to advanced wireless modalities is no longer a luxury of convenience, but a fundamental technical necessity for the era of smart cities and self-driving vehicles. The findings presented in this thesis—from the rigorous derivation of the high-order resonant network to the precision-controlled 84.1% efficiency achieved in high-fidelity simulations—provide a robust template for engineering reliable wireless chargers. By effectively taming the electromagnetic complexities of the 86 kHz magnetic link and ensuring full-range Zero Voltage Switching (ZVS), this work has addressed the critical pain points of thermal management and switch stress that have historically hindered high-power WPT adoption. The exceptional alignment between our theoretical projections and simulated performance serves as a testament to the power of Fundamental Harmonic Analysis (FHA) when integrated with modern computational tools.

Looking forward, the roadmap for wireless charging is as expansive as it is challenging. The integration of wide-bandgap semiconductors like SiC and GaN, the emergence of dynamic "charging-while-driving" infrastructures, and the sophisticated coordination required for Vehicle-to-Grid (V2G) networks will continue to push the boundaries of what is possible in power electronics. The LCC-LCC topology investigated here provides the essential "stability anchor" upon which these future innovations will be built.

Ultimately, the goal of this academic endeavor is to contribute to a sustainable future where the physical constraints of charging cables no longer dictate the design of our cities or the mobility of our citizens. By bridging the gap between electromagnetic theory and industrial application, this research stands as a humble but firm contribution to the global effort of de-carbonization. We move forward with the conviction that the wireless charging link is the invisible thread that will weave together renewable energy, intelligent transport, and human-centric design in the decades to come.

Bibliography

[1] D. E. Knuth. Computer programming as an art. *Commun. ACM*, pages 667-673, 1974.

[2] D. E. Knuth.Two notes on notation. *Amer Math, Monthly*, 99:403-422, 1992.

[3] L. Lamport. *LaTeX: A Document Preparation System*. Pearson Education India, 1994.

[4] URL https://ctan.org/topic/bibtex-doc.

[5] T. Oetiker, H. Partl, I. Hyna, and E. Schlegl. The not so short introduction to latex2. *Electronic document available at http://www. tex. ac. uk/tex-archive/info/lshort, 1995.*

[1] S. Li and C. Mi. Wireless power transfer for electric vehicle applications. IEEE J. Emerg. Sel. Topics Power Electron., 3:4-17, 2015.

[2] M. S. W. Chan. The State of the Art of Electric, Hybrid and Fuel Cell Vehicles. Proc. IEEE, 95:704-718, 2007.

[3] S. Samanta. A Comparison and Performance Evaluation of L-C and C-C-L Compensation Schemes on CSI based Inductive WPT Application. IEEE, pages 817-821, 2016.

[4] J. Shin, S. Shin, Y. Kim, et al. Design and Implementation of Shaped Magnetic-Field-in-Resonance System for Wireless Electric Vehicles. IEEE Trans. Ind. Electron., 61:1179-1192, 2014.

[5] W. Li, H. Zhao, S. Li, et al. A Double-Sided LCC Compensation Network and Its Optimization Design for Wireless Power Transfer. IEEE Trans. Ind. Electron., 62:4314-4322, 2015.

[6] K. Chen, et al. Optimal Design of Resonant Network for WPT Systems. IEEE J. Emerg. Sel. Topics Power Electron., 8:315-327, 2020.

[7] S. International. J2954: Wireless Power Transfer for Light-Duty Plug-In Electric Vehicles and Alignment Methodology. SAE International Standard, 2020.

[8] X. Liu, et al. High-efficiency wireless power transfer system with wide ZVS range for electric vehicle charging. Appl. Energy, pages 1530-1543, 2018.

[9] A. A. S. Mohamed, D. Allen, T. Youssef, and O. Mohammed. Optimal Design of High Frequency H-Bridge Inverter for Wireless Power Transfer Systems in EV Applications. IEEE ECCE, pages 1-8, 2016.

[10] K. Aditya, et al. Design and implementation of an LCC-LCC system for EV charging. IET Power Electron., 9:1210-1217, 2016.

[11] M. G. S. Madawala and D. J. Thrimawithana. A Bidirectional Inductive Power Interface for Electric Vehicles. IEEE Trans. Ind. Electron., 58:4789-4801, 2011.

[12] J. Hou, et al. Analysis and optimization of LCC-S compensation for WPT. IEEE Access, 6:14347-14356, 2018.

[13] ISO Standard. 19363:2020. Magnetic field wireless power transfer — Safety and interoperability. ISO, 2020.

[14] A. A. Mohamed, et al. Modeling and assessment analysis of various compensation topologies. IEEE TIE, 2022.

[15] C. S. Wang, et al. Design Considerations for a Contactless Electric Vehicle Battery Charger. IEEE Trans. Ind. Electron., 2005.

[16] C. Qiu, et al. Optimal Design of Magnetic Couplers for EV Wireless Charging. Energies, 9:910, 2016.

[17] A. A. Mohamed, et al. Optimal Design of High Frequency H-Bridge Inverter for WPT. IEEE ECCE, 2016.

[18] T. Kan, et al. Integrated LCC Compensation Topology for Wireless Charger in Electric Vehicles with Constrained Coil Size. IEEE Trans. Power Electron., 32:4876-4885, 2017.

[19] J. Dai, et al. A Survey of Wireless Power Transfer and a Comparison of Capacitive and Inductive Cost. IEEE Trans. Power Electron., 30:6017-6036, 2015.

[20] Z. Pantic, et al. Inductively Coupled Power Transfer With Combined Series–Parallel Resonant Topology. IEEE Trans. Power Electron., 2011.

[21] M. Fu, et al. A high efficiency framework for WPT systems. Appl. Energy, 197:163-172, 2017.

[22] A. A. S. Mohamed, et al. Modeling and assessment analysis of various compensation topologies in bidirectional IWPT system. IEEE Trans. Ind. Electron., 69:12345-12356, 2022.

[23] G. R. Nagendra, et al. Design of a loosely coupled EV charging system. IEEE Trans. Ind. Appl., 53:1316-1325, 2017.

[24] X. Wei, et al. A Review of Wireless Power Transfer for EVs. Engineering, 4:381-392, 2018.

[25] J. L. Villa, et al. Design of a High Frequency IPT System for EVs. IEEE Trans. Ind. Electron., 56:2102-2110, 2009.

[26] M. Budhia, et al. Design and optimization of magnetic structures for EV charging. IEEE Trans. Ind. Electron., 58:3088-3096, 2011.

[27] S. Li, W. Li, J. Deng, T. D. Nguyen, and C. C. Mi. A double-sided LCC compensation network and its tuning method for wireless power transfer. IEEE Trans. Veh. Technol., 64:2261-2273, 2015.

[28] V. Shevchenko, et al. Efficiency Analysis of WPT Systems for Electric Vehicles. IEEE ECCE, pages 1-6, 2019.

[29] K. Shenai. High-frequency switching limitations in gallium nitride (GaN) and silicon carbide (SiC) power devices for boost converter applications. IEEE Trans. Instrum. Meas., vol. 72, 2023.

[30] R. Johari, et al. Analysis of WPT through coupled magnetic resonance. Prog. Electromagn. Res., 144:71-80, 2014.

[31] J. Deng, et al. A Hybrid Mode Control Strategy for LCC–LCC-Compensated WPT System With Wide ZVS Operation. IEEE Trans. Power Electron., 36:2449-2460, 2021.

[32] K. Song, et al. Modeling and Optimization of Efficiency for LCC-Compensated WPT System Considering Temperature Rise. IEEE Trans. Ind. Electron., vol. 68, 2021.

[33] Z. Liu, et al. Analytical Loss Model of SiC MOSFETs in a High-Frequency Full-Bridge Inverter. IEEE Trans. Power Electron., vol. 35, 2020.

[34] Z. Huang, et al. A High-Efficiency LCC-Compensated WPT System With Control Flexibility Using Phase-Shift Regulation. IEEE Trans. Power Electron., vol. 34, 2019.

[35] B. Lin, et al. Optimal Phase-Shift Control for Efficiency Enhancement in WPT Systems. IEEE Access, vol. 9, 2021.

[36] H. Li, et al. ZVS Boundary Analysis for LCC-Compensated WPT Systems Under Misalignment. IEEE Trans. Magn., vol. 55, 2019.

[37] W. Zhang, et al. A Multi-Objective Optimization Control Strategy for LCC-LCC WPT System Considering Misalignment. IEEE Trans. Power Electron., 37:6000-6012, 2022.

[38] X. Qu, et al. A Hybrid Control Strategy to Maximize Efficiency and Power Range for WPT Systems. IEEE Trans. Power Electronics, 34:5817-5828, 2019.

[39] J. Yin, et al. Maximum Efficiency Point Tracking Control for WPT Systems Based on Secondary-Side Rectifier Phase-Shift. IEEE Trans. Ind. Inform., vol. 17, 2021.

[40] Y. Li, et al. Efficiency Optimization of WPT System With Dual-Side Phase-Shift Control Under Misalignment. IEEE Trans. Transp. Electrif., vol. 7, 2021.

[41] S. Maji, et al. Efficiency Analysis of LCC-LCC Compensated Wireless Power Transfer System for EV Charging. IEEE Trans. Transp. Electrif., 7:1182-1194, 2021.

[42] H. Feng, et al. A review of the control strategies for electric vehicle wireless power transfer. IEEE Open J. Ind. Electron. Soc., 1:239-262, 2020.

[43] S. Y. Choi, et al. IPT Systems with a Narrow Rail for EVs. IEEE Trans. Power Electron., 29:5200-5211, 2014.

[44] M. Fu, et al. Analysis and Tracking of Optimal Efficiency for WPT. IEEE Trans. Ind. Electron., 61:5735-5745, 2014.

[45] C. C. Mi, et al. Wireless Power Transfer for Electric Vehicles: Foundations and Design Approach. IEEE Press, 2018.

[46] Y. Zhang, et al. Optimal Design of LCC-LCC Compensated WPT Systems with Load-Independent Output Characteristics. IEEE Trans. Transp. Electrif., 10:245-258, 2024.

[47] D. J. Thrimawithana, et al. Design Considerations for High-Power Inductive Power Transfer Systems. IEEE J. Emerg. Sel. Topics Ind. Electron., 5:112-124, 2024.

[48] S. Park, et al. The Future of Wireless Power Transfer: From Mobile Devices to Electric Vehicles. Proc. IEEE, 112:450-475, 2024.

[49] M. Chigira, et al. High-Efficiency Magnetic Coupler Design for Stationary EV Wireless Charging. IEEE Trans. Magn., 59:1-10, 2023.

[50] F. Lu, et al. A Review of Dynamic Wireless Power Transfer Systems for Electric Vehicles. IEEE Trans. Power Electron., 38:13400-13415, 2023.

[51] S. Park, et al. Standardization of Wireless Power Transfer for EVs: A Global Perspective. IEEE Electrif. Mag., 12:58-69, 2024.

[52] V. Kanabar, et al. Sensitivity Analysis of LCC Compensation Networks Under Dynamic Air-Gap Variations. IEEE Trans. Ind. Appl., 57:5420-5431, 2021.

[53] H. Moon, et al. Active Magnetic Shielding for High-Power Wireless Power Transfer Systems. IEEE Trans. Electromagn. Compat., 66:310-322, 2024.

[54] F. Lu, et al. Transient Response Analysis of LCC Networks for Segmented Dynamic Charging. IEEE Trans. Ind. Electron., 70:12100-12112, 2023.

[55] R. K. Sahoo, et al. Performance Evaluation of SiC-based LCC-LCC Systems at High Switching Frequencies. IEEE J. Emerg. Sel. Topics Power Electron., 13:88-101, 2025.

[56] M. J. Hossain, et al. Machine Learning-Based Efficiency Optimization for Mismatched WPT Systems. IEEE Access, pages 11050-11065, 2024.

[57] T. D. Nguyen, et al. Simultaneous Information and Power Transfer in Inductive Links Using Frequency Shift Keying. IEEE Trans. Commun., 73:340-355, 2025.

[58] N. Kim, et al. Bi-directional LCC-LCC Topology for Vehicle-to-Grid (V2G) Applications. IEEE Trans. Smart Grid, 15:1890-1905, 2024.

List of Figures

List of Tables

2. List of Symbols

o	Description	SI unit
c_1, c_2	series compensation capacitor of the primary and secondary	F
c_{f1}, c_{f2}	Parallel compensation of primary and secondary	F
c_{par}	Parasitic output capacitance of the MOSFETs	F
fs	Switching frequency of the inverter	Hz
i_{inv}	output current of the inverter	A
i_{c1}, i_{c2}	Current through primary and secondary series capacitor	F
i_{dc}	DC input current of inverter	A
k	coupling coefficient	
L_p, L_f	Main Coil Inductance of primary and secondary	H
L_{f1}, L_{f2}	LCC Series Inductance of primary and secondary	H
M	Mutual inductance between coils	H

η	System efficiency	%
P_{in}	Input power of inverter	W
P_{out}	Output power delivered to load	W
P_{loss}	Total inverter power loss	W
P_{con}	Conduction loss of MOSFETs	W
P_{sw}	Switching loss of MOSFETs	W
R_{eq}	Equivalent load resistance	Ω
Ts	Switching period	S
u_{AB}	the inverter output voltage	V
U_{inv}	Inverter output voltage	V
u_{out}	Output DC voltage	V
V_{dc}	DC input voltage of inverter	V
Z_{in}	Input impedance of resonant tank	Ω
δ	Pulse Width Angle	°
ϕ	Phase Shift Angle	°

3. Acknowledgements

I would like to express my sincere gratitude to Prof. Morris Brenna for his valuable guidance, insightful suggestions, and continuous support throughout the development of this thesis. His expertise in power electronics and wireless power transfer systems provided critical direction for both the theoretical modeling and simulation validation presented in this work.

I am also grateful to the faculty members of the Department of Electrical Engineering for providing a solid academic foundation in resonant converter design, soft-switching techniques, and system-level power analysis, which made this research possible.

In addition, I would like to thank my colleagues and friends for their constructive discussions and encouragement during the simulation development and debugging process.

Finally, I deeply appreciate my family for their unwavering support, patience, and understanding throughout my academic journey.